

Fog and Cloud Induced Aerosol Modification Observed by AERONET

T.F. Eck^{1,2}, B.N. Holben², J.S. Reid³, D.M. Giles^{4,2}, M. A. Rivas⁵, R.P. Singh⁶, S.N. Tripathi⁷, C.J. Bruegge⁸, S.E. Platnick², G.T. Arnold^{9,2}, N.A. Krotkov², S.A. Carn¹⁰, A. Sinyuk^{4,2}, O. Dubovik¹¹, A. Arola¹², J.S. Schafer^{4,2}, P. Artaxo¹³, A. Smirnov^{4,2}, H. Chen¹⁴, and P. Goloub¹¹

1 Universities Space Research Association, Columbia, MD, USA

2 NASA Goddard Space Flight Center, Greenbelt, MD, USA

3 Naval Research Laboratory, Monterey, CA, USA

4 Sigma Space Corporation, Lanham, MD, USA

5 Universidad de Tarapaca, Arica, Chile

6 Chapman University, Orange, CA, USA

7 Indian Institute of Technology Kanpur, Kanpur, India

8 NASA/ Jet Propulsion Laboratory, Pasadena, CA, USA

9 Science Systems Applications Inc., Lanham, MD, USA

10 Michigan Technological University, Houghton, MI, USA

11 Universite de Lille, Villeneuve d'Ascq, France

12 Finnish Meteorological Institute, Kuopio, Finland

13 University of São Paulo, São Paulo, Brazil

14 Chinese Academy of Sciences, Beijing, China

Submitted to Journal of Geophysical Research - Atmospheres

AGU Index Terms: 0305, 0345, 0360

1 **Abstract.** Large fine mode (sub-micron radius) dominated aerosols in size distributions retrieved
2 from AERONET have been observed after fog or low-altitude cloud dissipation events. These
3 column-integrated size distributions have been obtained at several sites in many regions of the
4 world, typically after evaporation of low altitude cloud such as stratocumulus or fog. Retrievals
5 with cloud processed aerosol are sometimes bimodal in the accumulation mode with the larger
6 size mode often $\sim 0.4 - 0.5 \mu\text{m}$ radius (volume distribution); the smaller mode typically ~ 0.12 to
7 $\sim 0.20 \mu\text{m}$ may be interstitial aerosol that were not modified by incorporation in droplets and/or
8 aerosol that are less hygroscopic in nature. Bimodal accumulation mode size distributions have
9 often been observed from in situ measurements of aerosols that have interacted with clouds, and
10 AERONET size distribution retrievals made after dissipation of cloud or fog are in good
11 agreement with particle sizes measured by in situ techniques for cloud-processed aerosols.
12 Aerosols of this type and large size range (in lower concentrations) may also be formed by cloud
13 processing in partly cloudy conditions and may contribute to the ‘shoulder’ of larger size
14 particles in the accumulation mode retrievals, especially in regions where sulfate and other
15 soluble aerosol are a significant component of the total aerosol composition. Observed trends of
16 increasing aerosol optical depth (AOD) as fine mode radius increased suggests higher AOD in
17 the near cloud environment and therefore greater aerosol direct radiative forcing than typically
18 obtained from remote sensing, due to bias towards sampling at low cloud fraction.

19

20 **1. Introduction.**

21 Aerosol interactions with clouds are currently the largest source of uncertainty in assessment
22 of the anthropogenic aerosol radiative forcing on climate [IPCC, 2007]. This pertains primarily
23 to how aerosols modify cloud properties such as albedo [Twomey, 1977] and lifetime [Albrecht,
24 1989], and for absorbing aerosol particles the semi-direct effect of suppression of convection
25 [Hansen *et al.*, 1997, Koren *et al.*, 2005]. However, the related modification of aerosol properties
26 by interaction with clouds is also of significant importance in accurately assessing aerosol
27 evolution and direct radiative forcing. Globally the majority of aerosol particles are located in the
28 planetary boundary layer (typically lowest 1-3 km), therefore when low altitude non-
29 precipitating clouds (or fog) are coincident with or interact with this aerosol layer then the
30 potential for cloud-aerosol interactions is maximized. Aerosol particles may be modified by
31 clouds from hygroscopic growth in high relative humidity conditions within the cloud, or in the

32 near-cloud enhanced humidity environment [Radke and Hobbs, 1991]. Additionally, aerosol
33 particles may serve as cloud condensation nuclei (CCN) and subsequent aqueous phase
34 chemistry may result in modified aerosol properties of the particles that remain after evaporation
35 of the cloud droplet, i.e. cloud processed aerosols [Hoppel et al., 1994; Alkezweeny, 1995;
36 Lelieveld and Heintzenberg, 1992; Lu et al., 2003; Hegg et al., 2004]. Those particles that have
37 served as CCN and subsequently exhibited an increase in size and mass are also sometimes
38 called cloud residue. Furthermore, new particle formation has also been observed in cloud
39 environments [Hoppel et al., 1994]. Ultimately the processing of aerosol particles in clouds
40 results in larger particle sizes and increased soluble components.

41 Several recent studies suggest changes in aerosol optical properties by clouds or in the
42 vicinity of clouds. *Twohy et al.* [2009] analyzed in situ aircraft data from INDOEX over the
43 northern Indian Ocean and found relative humidity increased within ~1 km of small low altitude
44 marine cumulus, and this resulted in increases of about 40-80% in aerosol scattering as a result
45 of hygroscopic growth. *Li et al.* [2011] made in situ measurements of aerosols from a mountain
46 observatory at ~1.5 km altitude in northeastern China during 4 days in April 2010. Their
47 observations were made under highly polluted aerosol conditions and found significantly larger
48 radius for cloud residue aerosols versus interstitial aerosol (~0.22 μm versus ~0.4 μm , for
49 number size distributions), and the number of particles decreased by ~50% during cloud
50 formation demonstrating how efficiently aerosol particles were incorporated into cloud droplets.
51 They also found that ~92% of the cloud residue particle composition was dominated by sulfate
52 and soluble organic matter salts. *Zhang and Tie* [2011] measured 75% conversion of sulfur
53 dioxide from gas to aqueous phase during a fog event in polluted conditions, in the same region
54 of northeastern China, suggesting that SO_2 has greater solubility than had been previously
55 thought.

56 Several studies have used lidar observations to investigate the aerosol environment in the
57 proximity of clouds. *Su et al.* (2008) used HSRL lidar from aircraft to investigate the near cloud
58 aerosol environment for three cases of low altitude clouds (<3 km). They found enhancement of
59 aerosol optical depth (AOD) by ~8-17% within ~100 meters of clouds in comparison to
60 measurements made 4.5 km from clouds. They suggest that the observed increases in backscatter
61 and extinction coefficients near clouds could be explained by both humidification and cloud
62 processing of aerosols. Analysis of satellite lidar data from CALIPSO by *Tackett and*

63 *DiGirolamo* [2009] showed enhanced backscatter near to the cloud edge for western Atlantic
64 trade wind cumulus (single layer), which they suggested was best explained by increased aerosol
65 radius and reduced number size distribution. Additionally, an analysis of CALIPSO data over
66 oceans by *Varnai and Marshak* [2011] found increased backscatter and increased particle size in
67 a transition zone of ~15 km around clouds over all oceans, with near cloud enhancements
68 strongest at low altitudes.

69 An analysis of the relationship between cloud fraction and AERONET direct sun
70 measurements of AOD, for a site in the US Great Plains region (Oklahoma) was carried out by
71 *Jeong and Li* (2010). Their study showed increasing AOD as cloud fraction increased, with only
72 about 25% of the increase attributed to humidification, while the bulk of the increase was likely
73 due to a combination of cloud processing of aerosols, new particle genesis and atmospheric
74 dynamics. Additionally, they also found that in situ aircraft measured AOD (vertically integrated
75 extinction coefficients) at the same site and time interval also showed increasing AOD as cloud
76 cover increased, thereby reducing the possibility that any significant amount of the
77 sunphotometer measured increases in AOD as a function of cloud fraction were due to cloud
78 contamination.

79 In the current study we analyze aerosol size distribution retrievals from almucanatar scans
80 made by AERONET sun-sky radiometers in specific situations where extensive fog or low
81 altitude cloud layers have recently dissipated (evaporated). These are cases where at least a
82 portion of both the aerosol layer and fog/ cloud layer were coincident in vertical profile thereby
83 resulting in significant probability for cloud-aerosol interaction. Cases from many different
84 regions of the world are shown for interaction between primarily pollution (urban-industrial
85 type) aerosols and cloud or fog.

86

87 **2. Instrumentation and Methodology**

88 **2.1 AERONET Instrumentation**

89 The CIMEL Electronique CE-318 sun-sky radiometer measurements were made with
90 instruments that are a part of the AErosol RObotic NETwork (AERONET) global network.
91 These instruments are described in detail by *Holben et al.* [1998], however a brief description is
92 given here. The automatic tracking Sun and sky scanning radiometers made direct Sun
93 measurements with a 1.2° full field of view every 15 minutes at 340, 380, 440, 500, 675, 870,

94 940, and 1020 nm (nominal wavelengths). However for the Beijing site the version of the
95 CIMEL installed there most years had only the 440, 675, 870 and 1020 nm channels for AOD
96 measurement. The direct sun measurements take ~ 8 seconds to scan all 8 wavelengths (repeated
97 three times within a minute), with a motor driven filter wheel positioning each filter in front of
98 the detector. These solar extinction measurements are used to compute aerosol optical depth
99 (AOD or τ_a) at each wavelength except for the 940 nm channel, which is used to retrieve total
100 column water vapor (or precipitable water) in centimeters. The filters utilized in these
101 instruments were ion assisted deposition interference filters with bandpass (full width at half
102 maximum) of 10 nm, except for the 340 and 380 nm channels at 2 nm. The estimated uncertainty
103 in computed τ_a , due primarily to calibration uncertainty, is ~ 0.010 - 0.021 for field instruments
104 (which is spectrally dependent with the higher errors in the UV; *Eck et al.* [1999]). *Schmid et al.*
105 [1999] compared τ_a values derived from 4 different solar radiometers (including an AERONET
106 sun-sky radiometer) operating simultaneously together in a field experiment and found that the τ_a
107 values from 380 to 1020 nm agreed to within 0.015 (rms), which is similar to our estimated level
108 of uncertainty in τ_a retrieval for field instruments. Only AERONET version 2 level 2 AOD data
109 have been analyzed, unless otherwise specified. The spectral aerosol optical depth data have
110 been screened for clouds following the methodology of *Smirnov et al.* [2000], which relies on the
111 higher temporal frequencies of cloud optical depth versus aerosol optical depth. The sky
112 radiances measured by the sun/sky radiometers are calibrated versus frequently characterized
113 integrating spheres at the NASA Goddard Space Flight Center, to an absolute accuracy of $\sim 5\%$
114 or better [*Holben et al.*, 1998].

115

116 **2.2 Inversion Methodology**

117 The CIMEL sky radiance measurements in the almucantar geometry (fixed elevation angle
118 equal to solar elevation and a full 360° azimuthal sweep) at 440, 675, 870, and 1020 nm (nominal
119 wavelengths) in conjunction with the direct sun measured τ_a at these same wavelengths were
120 used to retrieve optical equivalent, column integrated aerosol size distributions and refractive
121 indices. Using this microphysical information the spectral dependence of single scattering albedo
122 is calculated. The algorithm of *Dubovik and King* [2000] with enhancements detailed in
123 *Dubovik et al.* [2006] was utilized in these retrievals, known as Version 2 AERONET retrievals.
124 Only Version 2 and Level 2 quality assured retrievals [*Holben et al.*, 2006] are presented in this

125 paper, unless otherwise noted. The Version 2 AERONET algorithm determines the percentage of
126 spherical and spheroidal particles required to give the best fit to the measured spectral sky
127 radiance angular distribution. Further details on the Version 2 algorithm and the improved
128 specification of surface bidirectional reflectance can be found in *Dubovik et al.* [2006] and *Eck et*
129 *al.* [2008].

130 Almucantar sky radiance measurements were made at optical airmasses of 4, 3, 2, and 1.7 (75,
131 70, 60, 54 degrees solar zenith angle respectively) in the morning and afternoon, and once per
132 hour in between. In order to ensure sky radiance data over a wide range of scattering angles, only
133 almucantar scans at solar zenith angles greater than ~ 50 degrees are analyzed and presented here.
134 To eliminate cloud contamination from the almucantar directional sky radiance data AERONET
135 requires the radiances to be symmetrical on both sides of the sun at equal scattering angles, and
136 symmetric radiances from both sides are subsequently averaged. Directional sky radiance
137 measurements that are not symmetrical (due to cloud on one side or inhomogeneous aerosol
138 distribution) are eliminated, and the minimum number of measurements required in given
139 scattering angle ranges for a Level 2 retrieval are shown in *Holben et al.* [2006]. The stable
140 performance of the inversion algorithm was illustrated in sensitivity studies performed by
141 *Dubovik et al.* [2000] where the perturbations of the inversion resulting from random errors,
142 possible instrument offsets and known uncertainties in the atmospheric radiation model were
143 analyzed. Their work employed retrieval tests using known size distributions to demonstrate
144 successful retrievals of mode radii and the relative magnitude of modes for various types of
145 bimodal size distributions such as those dominated by a sub-micron accumulation mode or
146 distributions dominated by super-micron coarse mode aerosols. Although very few direct
147 comparisons of size distribution between in situ and AERONET retrievals have been made there
148 are several aerosol types in specific regions that have been or can be compared. For example,
149 *Reid et al.* (2005) presents a table where the volume median radius of smoke from various major
150 biomass burning regions (South America, southern Africa, North America (boreal, temperate))
151 are compared. For all three of these regions, the volume median diameters of the in situ versus
152 the AERONET retrievals are often within $\sim 0.01 \mu\text{m}$ of each other. Similarly, for fine mode
153 pollution in the Arabian Sea during INDOEX, *Clarke et al.* [2002] presented lognormal fits of
154 volume size distributions from aircraft and ship in situ instrument measurements that showed
155 average accumulation mode volume peak radius values of $0.17 \mu\text{m}$ to $0.18 \mu\text{m}$ with geometric

156 standard deviations of 1.43 (aircraft) and 1.51 (ship) for observations made under high aerosol
157 scattering conditions. This compares well with retrievals made at Kaashidhoo Island, Maldives
158 (in the same region), when $AOD(440\text{ nm}) > 0.4$, of $0.18\ \mu\text{m}$ median radius and width of 1.49
159 (AERONET Version 2 averages from 1998-2000). For larger sub-micron sized aerosols, *Eck et al.*
160 *al.* [2010] discussed the relatively close agreement for Pinatubo stratospheric aerosol
161 observations of $\sim 0.56\ \mu\text{m}$ peak volume radius from AERONET retrievals to $0.53\ \mu\text{m}$ effective
162 radius from in situ stratospheric aircraft measurements, as reported by *Pueschel et al.* [1994]. In
163 the coarse mode (super-micron radius), *Reid et al.* [2006] and *Reid et al.* [2008] showed
164 excellent agreement between in situ measured size and AERONET retrievals for sea salt and
165 desert dust, respectively. Similarly, *Johnson and Osborne* [2011] have shown good agreement
166 between aircraft in situ measured size distributions and AERONET retrievals for coarse mode
167 dust in the Sahel region of West Africa.

168

169 **3. Results and Discussion**

170 **3.1 Kanpur, India**

171 The Kanpur AERONET site in India is located immediately to the northwest of Kanpur, an
172 industrial city with population ~ 5 million in 2009. The Indo-Gangetic Plain region where Kanpur
173 is located is a major emission source of pollution aerosol from the combustion of fossil fuels and
174 biofuels [*Singh et al.*, 2004; *Novakov et al.*, 2000; *Venkataraman et al.*, 2005; *Prasad et al.*,
175 2006]. Also in spring and early summer the aerosol type dynamics at Kanpur was strongly
176 influenced by desert dust advected eastward from the Thar desert of the India/Pakistan border
177 region and from arid regions farther west in the Middle East [*Dey et al.*, 2004; *Chinnam et al.*
178 2006; *Prasad and Singh*, 2007; *Guatam et al.*, 2009]. Analysis of aerosol Fine Mode Fraction
179 (FMF) of AOD versus Angstrom exponent (440-870 nm) from a previous paper [*Eck et al.*, 2010]
180 for Kanpur, India showed a multi-year (2002-2006) climatology based on almucantar retrievals
181 of FMF. As identified in Figure 1, there is a small cluster of outlier observations that have
182 relatively low Angstrom exponent (< 1.0) at high fine mode fraction of AOD (> 0.90 at 440 nm).
183 All of the outlier cases in this plot occurred during the month of January, when fine mode
184 pollution aerosols dominate [*Eck et al.*, 2010]. When these dates were examined in detail, it was
185 observed for all of these cases that MODIS satellite images showed low cloud or fog (fog is
186 cloud that extends to the earth's surface) either over or near to the Kanpur site location at the

187 time of the morning Terra satellite overpass, with the fog/cloud having dissipated or partially
188 dissipated by the time of the early afternoon Aqua satellite overpass. It is well known that fog
189 frequently occurs in the Indo-Gangetic plain in the winter months and is typically associated with
190 high aerosol concentrations [Jenamani, 2007; Gautam et al., 2007; Badarinath et al., 2009;
191 Tripathi et al., 2006; Tare et al., 2006; Baxla et al., 2009], affecting the lives of millions of
192 people in the region due to cancellation of flights, late running trains, and poor visibility. MODIS
193 satellite images for one of these cases, January 5, 2006, are shown in Figure 2. Weather
194 station observations obtained from Russia's Weather Server–Weather Archive
195 (<http://meteo.infospace.ru/wcarch/html/index.sht>) on this date from nearby Lucknow (~60 km
196 northeast of Kanpur) indicated patches of shallow fog with 94% surface relative humidity and
197 0.5 km visibility at 0300 UTC, and at 0600 UTC mist was observed with cloud base height at
198 150 meters and 90% cloud cover, while there were no clouds noted from 09 through 18 UTC. On
199 this day satellite imagery shows that an extensive area of bright white cloud/fog is located
200 immediately adjacent and to the north of the Kanpur site at the Terra overpass time of 0515 UTC
201 while most of this fog/cloud has dissipated by about 0820 UTC (3 hours later) at the time of the
202 Aqua overpass. A relatively uniform gray haze is seen in the Aqua image in the region
203 surrounding Kanpur after the dissipation of the fog/cloud.

204 The cloud screened spectral AOD observations for this day show that AOD (440 nm) was
205 approximately 0.60. The two almucantar retrievals (level 2.0) were made at 0837 UTC and 1006
206 UTC, when the Angstrom exponent (440-870 nm) was ~0.84 and ~1.0, respectively. The aerosol
207 volume size distribution retrievals from these two almucantar scans are shown in Figure 3. The
208 bimodal nature of the accumulation mode (radius < 1 micron) seen in these cases is not very
209 commonly observed in AERONET retrievals. Exceptions include aged volcanic aerosol in the
210 stratosphere (from Mt. Pinatubo, for example) and sometimes dust from certain source regions
211 such as the Bodele depression, which both had a volume distribution mode peak radius of ~0.60
212 micron [Eck et al. 2010]. The larger mode in this Kanpur case shows a peak radius of ~0.45
213 microns, with the smaller of the two accumulation modes peaking at ~0.15 to 0.20 microns. It is
214 noted that the coarse mode AOD (computed from radius > 0.99 μm) for these retrievals is only
215 0.015 to 0.022 (wavelength independent), relatively insignificant compared to the fine mode
216 AOD. In situ measured aerosol size distributions have shown bimodality of the accumulation
217 mode in cases where at least some of the particles have been cloud processed. Hoppel et al.

218 [1994] measured aerosol number size distributions from an airship in close proximity to a stratus
219 cloud deck off of the coast of Oregon. These size distributions exhibited a distinct bimodality in
220 the accumulation mode that Hoppel et al. attributed to cloud processing of aerosols and in-cloud
221 conversion of sulfur dioxide gas to sulfate particles, which formed the larger of the two modes,
222 and the interstitial aerosols (not interacting with cloud) comprising the smaller of the modes. *Das*
223 *et al.* [2008] also measured bimodal submicron aerosol size distributions and an increase in
224 accumulation mode radius for aerosols that had interacted with fog in the Indo-Gangetic Plain of
225 India. In Figure 3 it is seen that the size distribution retrieved closer to the time of the fog
226 dissipation (evaporation) shows a greater contribution of the $\sim 0.45 \mu\text{m}$ radius mode than
227 retrieved ~ 1.5 hours later, perhaps due to decay or dissipation of the cloud processed aerosol, and
228 conversely a larger contribution (and smaller radius) of the interstitial aerosol mode perhaps due
229 to drying of humidified aerosol and emission and/or creation of fresh aerosols. The smaller of the
230 two modes may also be aerosol that had no interaction with the fog, perhaps aerosol that was
231 located at an altitude above the fog layer. *Dall'Osto et al.*, [2009] measured ambient aerosol
232 sizes in association with a fog event in London, and data for the largest mode measured are
233 reproduced in Figure 4 (with additional conversion to volume distribution). The large particles
234 shown in this figure are composed of hydroxymethanesulphonate (HMS), which is a chemical
235 species that is only formed in aqueous phase chemistry and therefore a valuable tracer for aerosol
236 processing by cloud or fog. It is noted that the size of these HMS particles formed in the London
237 fog event (peak volume radius of $\sim 0.45\text{-}0.50 \mu\text{m}$) are essentially the same as the larger of the
238 two accumulation modes observed over Kanpur after fog dissipation (Figure 3).

239 In addition to aerosol size distribution modification by fog/cloud interaction, the AERONET
240 retrievals also suggest that the aerosol absorption properties are modified. Figure 5 shows the
241 retrieved aerosol single scattering albedo (SSA) in visible wavelengths (440 and 675 nm) as a
242 function of fine mode volume median radius for all almucanatar retrievals made during the
243 month of January at the Kanpur site. There is a clear trend of increasing SSA as fine mode radius
244 increases. The largest of these fine mode radius cases, with radius $> 0.25 \mu\text{m}$, are mostly
245 fog/cloud interaction cases, and show a nearly linear increase in SSA as radius increases. These
246 larger size cloud processed aerosols would likely contain more water and sulfate, both of which
247 are non absorbing, and the increased radius of the aerosols also increases the scattering
248 efficiency, thereby increasing the single scattering albedo. Figure 5 also shows that there is a

249 distinct trend of increasing SSA as radius increases for aerosol of radius $<0.25 \mu\text{m}$, likely due to
250 particle growth by coagulation and hygroscopic growth, also resulting in more efficient
251 scattering at larger radius in combination with either nearly constant or lower imaginary
252 refractive index.

253 The relationship between low altitude cloud fraction (in conjunction with cloud optical depth;
254 COD) and aerosol radius for dates where almucantar retrievals were made in January at Kanpur
255 were investigated. Data from January of both 2003 and 2006 were selected since these years had
256 the most cases with very large fine mode aerosol radius retrieved from AERONET. Figure 6
257 shows the product of the low cloud fraction (> 600 mb cloud top pressure) times low cloud
258 optical depth from the MODIS cloud algorithm [Platnick *et al.*, 2003] at the Terra satellite
259 overpass time of mid-morning. The retrieved radius values are from almucantar scans made after
260 the fog/low cloud had dissipated, and are daily averages of all retrievals made in a given day.
261 Figure 6 shows a rapid increase in accumulation mode aerosol radius as the low cloud fraction*
262 COD increases, consistent with fog/cloud processing of aerosol, since at higher low cloud optical
263 depths and fractions it is likely that the fog layer is deeper and/or denser, thereby increasing the
264 probability of cloud/fog droplet interaction with the aerosols over a greater vertical extent of the
265 boundary layer.

266

267 **3.2 Arica, Chile**

268 The Arica AERONET site (18.47° S, 70.31° W, 25 m elevation) is located within less than
269 0.5 km of the Pacific Ocean coast in northern Chile in the small city of Arica (population
270 $\sim 200,000$). Arica is situated approximately 140 km southeast from Ilo, Peru which is the location
271 of a large copper smelter near to the coast, one of the largest single point sources of sulfur
272 dioxide on Earth [Carn *et al.*, 2007 and references therein]. The region of Arica, Ilo and the
273 surrounding Atacama Desert is one of the driest on Earth, with extremely low annual rainfall
274 (~ 0.8 mm average at Arica). Large emissions of SO_2 from Ilo have been observed from the
275 Ozone Monitoring Instrument (OMI) satellite sensor [Carn *et al.*, 2007]. Most of the Peru coast
276 and the central through northern Chilean coasts are adjacent to one of the largest and most
277 seasonally persistent stratocumulus cloud fields in the world [Klein and Hartmann, 1993;
278 Bretherton *et al.*, 2004]. Kuang and Yung [2000] have analyzed data from the Total Ozone
279 Mapping Spectrometer (TOMS) on the Nimbus-7 satellite, showing higher stratocumulus cloud

280 reflectance adjacent to Ilo and another near coastal smelter in Peru, thereby suggesting possible
281 indirect aerosol effects of increased cloud droplet number, resulting in higher cloud albedo.

282 *Chand et al.* [2010] measured aerosol properties further south on the Chilean coast ($\sim 25^{\circ}$ S)
283 at 690 meters altitude and found that sulfate was the dominant identified submicron species,
284 constituting 40% of the dry mass. For data sampled in situ from aircraft at 20° S westward off the
285 coast of Chile in the marine stratocumulus region, *Allen et al.* [2011] found cloud droplet number
286 well correlated with accumulation mode aerosol number and consistent with complete activation
287 of $0.15 \mu\text{m}$ diameter number distribution accumulation mode aerosols.

288 The marine stratocumulus cloud cover often overlays the Arica site in the morning and
289 sometimes though the mid-afternoon, typically evaporating as the underlying land surface heats
290 up. An example of an almucantar retrieval made after the dissipation of the stratocumulus layer
291 over the site is shown in Figure 7. This case was observed on July 13, 2008, when cloud
292 prevented direct sun measurement of AOD until the last two hours of the AERONET daily
293 measurement sequence in late afternoon. The MODIS images on this date show 100% cloud
294 cover with high visible reflectance over the ocean and Arica site at Terra overpass, and
295 remaining similar over the ocean at Aqua overpass 3 hours later, but evaporating over the land at
296 that time. The 440 nm AOD during the almucantar scan averaged 0.58 and the $\alpha_{440-870}$ was 0.77.
297 Similar to the size distribution retrievals at Kanpur shown in Figure 3, Figure 7 shows a bimodal
298 submicron size distribution with the largest of the two modes having a volume radius peak of
299 $\sim 0.48 \mu\text{m}$. The smaller of the two modes has a peak at $\sim 0.16 \mu\text{m}$, and the volume median radius
300 of combined submicron modes is $0.33 \mu\text{m}$. The larger of the two modes is likely the result of
301 cloud processing of aerosol and the smaller possibly being composed of interstitial aerosol, or
302 aerosol with no interaction with the cloud layer (such a aerosol above or below cloud top
303 altitude). The coarse mode (super-micron radius) in this retrieval has an AOD of only ~ 0.03 ,
304 which is nearly spectrally constant from 440 to 1020 nm, resulting in the AOD fine mode
305 fraction of ~ 0.95 at 440 nm and ~ 0.91 at 870 nm. The retrieved single scattering albedo for this
306 case is ~ 0.99 (also spectrally neutral), and therefore very weakly absorbing which is typical of
307 most retrievals at Arica, where the average SSA is 0.98 for all wavelengths, from nearly 400
308 retrievals from 1998-2000, where $\text{AOD}(440 \text{ nm}) > 0.4$. This is consistent with the principal
309 aerosol sources in the Arica region, as the SO_2 emissions from copper smelting create sulfate
310 particles that are non-absorbing [*Haywood and Boucher, 2000*] and both sea salt and marine

311 biogenic sulfate particles (from dimethyl sulfide emission by phytoplankton) are also non-
312 absorbing.

313 Several studies [*Reid et al.*, 1999; *Eck et al.*, 1999; *Eck et al.*, 2001; *Eck et al.*, 2003] have
314 shown that there is significant curvature in the \ln AOD versus $\ln \lambda$ relationship for fine mode
315 dominated aerosol size distributions, and that this curvature increases as submicron particle
316 radius increases. The magnitude of the curvature is parameterized by $\alpha' = d\alpha/d \ln \lambda$ [*Eck et al.*,
317 1999] since there is typically a linear or near linear relationship between Angstrom Exponent and
318 $\ln \lambda$, from the ultraviolet through near infrared wavelengths. In Figure 8a we show the
319 relationship between the almucantar retrieved volume median radius of the fine mode and the
320 magnitude of α' computed from the 380 nm through 870 nm AOD measurements for all Arica
321 retrievals made from 1998-2008. A zero value of α' means that there is no curvature and that the
322 spectral AOD follow the linear or Angstrom relationship in \ln AOD versus $\ln \lambda$. Negative values
323 of α' typically occur when a significant coarse mode optical depth fraction exists, while positive
324 values occur for fine mode dominated size distributions, with α' increasing as accumulation
325 mode radius increases. The Arica retrieval shown in Figure 7 with the large cloud processed
326 mode has a large α' value of 1.49, indicating strong non-linearity in the AOD spectra induced by
327 large fine mode aerosols. Retrieved size distributions with submicron volume median radius of
328 $\sim 0.40 \mu\text{m}$ or higher are dominated by the cloud processed particles and have little contribution
329 from the smaller 'interstitial' size accumulation mode aerosol (or aerosol that had no interaction
330 with clouds, perhaps due to differing altitude). Many of the retrievals with volume median radius
331 range of $0.20 - 0.30 \mu\text{m}$ do not exhibit bimodality of the accumulation mode, but typically
332 exhibit larger width of the fine mode (fine mode width increased as fine modal radius increased
333 (correlation coefficient of 0.48)), including possibly more contribution of larger particles which
334 may have interacted with cloud droplets. Figure 8b shows the scatterplot relationship between
335 the aerosol optical depth and retrieved fine modal radius at Arica. There is an increasing trend of
336 AOD at 440 nm as fine mode radius increases, with correlation coefficient (r) of 0.48. This trend
337 may be due to several factors including an increase in coagulation rate as concentration increases
338 [*Colarco et al.*, 2004], aerosol humidification, and also due to cloud processing of aerosols to
339 larger sizes. When the particle number remains constant but the radius increases in the fine mode
340 there is a resultant significant increase in AOD due to an increase in light scattering efficiency.

341 Of course many other factors influence the relationship shown in Figure 8b, such as aerosol
342 concentrations, wind speed and resultant turbulent mixing, depth of the aerosol boundary layer,
343 aging of the aerosol, and distance from aerosol sources, among others, which may partially
344 account for the large amount of scatter in this plot.

345 The relationship between aerosol fine mode radius from AERONET and cloud fraction as
346 determined by MODIS satellite measurements at Arica was also investigated. Figure 9 shows the
347 annual variation in the retrieved volume median radius and the low cloud fraction (> 600 mb
348 cloud top pressure) retrieved from the MODIS cloud algorithm with Terra satellite measurements.
349 The MODIS cloud fraction is for a 1 by 1 degree latitude-longitude grid average with
350 midpoint of 18.5°S 71.5°W, therefore all over ocean, directly to the west of Arica. All
351 individual AERONET retrievals of fine mode radius from 1998-2008 are shown and the monthly
352 mean low cloud fractions computed from 2001-2009 data are also depicted. The months of June
353 through September exhibit the highest cloud fractions (>0.80) while the lowest fractions
354 occurred during the months of January through March (<0.40). There is correspondingly similar
355 seasonal trend in fine mode radius, which is most obvious in the lowest values over the annual
356 cycle. This general coincidence of annual cycle in low cloud fraction and fine mode radius is
357 consistent with the likelihood of cloud processing of the fine mode (largely sulfate) aerosol
358 and/or humidification growth in the higher relative humidity environment in the vicinity of the
359 clouds.

360 The previously mentioned copper smelter at Ilo, Peru had a significant upgrade in January
361 2007 in order to decrease the emissions of sulfur dioxide. In Figure 10a, the time series of
362 monthly mean AOD (500 nm) from 1998 to 2010 is shown, although a gap occurred in the data
363 from April 2004 through May 2007 due to a combination of logistics issues and technical
364 problems. Figure 10b shows the daily average SO₂ mass column amounts measured by the OMI
365 satellite instrument [Carn *et al.*, 2007] from September 2004 through 2010. Note that the highest
366 total column SO₂ were measured in 2006 through spring 2007, due to the additional source of the
367 Ubinas volcano eruptions upwind of Ilo. Unfortunately the AERONET data is missing when the
368 smelter upgrade occurred in 2007, however the significant decrease in AOD from May 2007
369 through January 2010 as compared to May 1998 through March 2004, strongly suggests that the
370 ~90% reduction in emissions from this single major source has had a significant impact on the
371 column integrated aerosol loading over the Arica site. There are only a few monthly mean AOD

372 (500nm) > 0.3 after May 2007 and none greater than 0.4, when prior to April 2004 there were
373 several months with relatively high AOD, including three months with ~0.5. Although the AOD
374 exhibited a significant decrease, the fine mode radius does not show a significant change, with
375 the linear regression showing a correlation coefficient (r) of only 0.10 (~1% of variance
376 explained). Therefore it appears that the frequency of cloud processing and/or humidification of
377 the aerosol over Arica may have remained relatively unchanged despite the significant drop in
378 aerosol concentrations.

379

380 **3.3 Fresno, California, USA**

381 The AERONET site in Fresno, CA is located near downtown Fresno, which is a city with a
382 population of ~1 million located near the center of the wide San Joaquin Valley of Central
383 California. Thick radiation fog frequently forms in the late fall and winter (the rainy season) after
384 the first significant rainfall. This fog often forms over a large area of the Central Valley bounded
385 by the mountains of the Coast Ranges in the west and the Sierra Nevada to the east. Aerosol and
386 aerosol precursor gases emitted in this region include urban, industrial, transportation and
387 agricultural sources [Chow *et al.*, 2006]. Airborne high spectral resolution lidar data from Feb
388 2007 in the San Joaquin Valley [Lewis *et al.*, 2010] showed a shallow aerosol layer of ~1 km
389 depth (constrained by temperature inversions), thereby increasing the likelihood that low altitude
390 cloud and especially fog may possibly interact with a significant fraction of the boundary layer
391 aerosol in this region.

392 Figure 11 is an Aqua MODIS image showing most of central California, adjacent Pacific
393 Ocean and part of Nevada on January 13, 2004 at 2110 UTC, with snow on the ground over high
394 elevations of the Sierra Nevada range. The majority of the Central Valley is covered in highly
395 reflective fog or low cloud, and the location of Fresno is indicated on the image. Observations
396 made at the Fresno airport on this date show cloud base at 75 m at 12 UTC (mist and 50% cloud),
397 at 800 m (mist and 100% cloud) at 18 UTC and at 3000 m at 00 UTC on Jan 14 (haze and 30%
398 cloud). AERONET observations showed cloud-free data for only the last hour of measurements
399 of the day, and Figure 12a is the almucantar scan size distribution retrieval made at 2332 UTC
400 (75° solar zenith), from approximately 2.4 hours after the MODIS image in Figure 11. The
401 bimodal accumulation mode size distribution observed in Figure 12a is very similar to those
402 observed in Kanpur and Arica, with the peak radius of the larger mode at $\sim 0.43 \mu\text{m}$ and the peak

403 radius of the smaller mode at $\sim 0.19 \mu\text{m}$ (total median fine mode radius was $0.28 \mu\text{m}$). The
404 Angstrom exponent (440-870) is also similar (1.06) to that shown for the other cases, and the
405 coarse mode aerosol optical depth determined from the retrieval is ~ 0.01 , resulting in spectral
406 fine mode fractions of the AOD of 0.96 at 440 nm and 0.92 at 870 nm. Several investigations
407 [*Whiteaker and Prather*, 2003; *Rao and Collett*, 1995; *Jacob et al.*, 1989; *Munger et al.*, 1986]
408 have measured the presence of hydroxymethanesulfonate in fog droplets and aerosols in the
409 Central Valley of California in winter, and *Dixon and Aasen* [1999] measured aerosol HMS at
410 other locations in the USA as well. As previously mentioned (Figure 4), HMS particles are a
411 tracer for aqueous phase aerosol processing in fog or cloud droplets and are of a large size, ~ 0.4 -
412 $0.5 \mu\text{m}$ radius. *Whiteaker and Prather* [2003] suggest that the formation rate of HMS
413 increases as pH increases, reaching a maximum late in the lifetime of the fog and that the
414 percentage of aerosol containing HMS reached a maximum of 40-50% following fog events at
415 Bakersfield, California (also in the Central Valley). *Herckes et al.* [2007] measured high pH
416 values in San Joaquin Valley fogs in winter, thus making them effective in oxidation of sulfur
417 dioxide and for production of HMS. Measurements of the size distribution of ambient particles
418 by *Whiteaker and Prather* [2003] showed a much higher frequency of particles containing HMS
419 with aerodynamic radius greater than $0.35 \mu\text{m}$ (continuing to $\sim 1 \mu\text{m}$ radius), therefore consistent
420 with the measurements of HMS particle size made by *Dall'Osto et al.* [2009] in London. *Fahey*
421 *et al.* (2005) in an analysis of San Joaquin Valley fog, simulated the mass size distribution of
422 sulfate aerosol utilizing two different fog process models and found that the particle size
423 distribution peaked at $0.38 \mu\text{m}$ radius, similar to in situ measurement results for ambient aerosols
424 containing HMS.

425 Size distribution retrievals showing bimodality on another date in Fresno, February 11, 2006
426 are shown in Figure 12b. The Fresno airport recorded mist at 12 UTC with 86% RH, and haze at
427 18 UTC with 64% RH (6 hourly report interval). The larger of the sub-micron modes (likely
428 cloud processed) shows a peak radius decreasing from ~ 0.50 to $\sim 0.45 \mu\text{m}$, while the smaller
429 mode also remained relatively constant at ~ 0.22 to $\sim 0.19 \mu\text{m}$ (this slight decrease of the smaller
430 mode may be related to decreasing RH) over the time interval of ~ 3 hours for these 5 almucantar
431 scans. Again the coarse mode (super-micron radius) AOD computed from these size distributions
432 was small, ~ 0.01 (all wavelengths), therefore relatively insignificant optically. The 440 nm AOD
433 decreased from ~ 0.43 at the time of the first scan shown to 0.31 at the time of the last scan, and

434 the $\alpha_{440-870}$ increased from ~ 1.08 to 1.27. These observations show the temporal dissipation of
435 the larger mode, which is consistent with estimates of the lifetime of HMS of a few hours after
436 fog events [Whitaker and Prather, 2003].

437 All of the individual AERONET retrievals of fine mode radius made at Fresno are shown
438 versus day of the year, from the time interval of 2002-2009, in Figure 13a. The majority of
439 retrievals with fine mode median radius $> 0.20 \mu\text{m}$ occurred from November through mid-March.
440 Also shown in this figure is the monthly mean low cloud fraction from Terra MODIS (cloud top
441 $> 600 \text{ mb}$), averaged over the 2001 through 2009 interval. The annual cycle of low cloud fraction
442 closely follows the annual cycle of fine mode radius with low cloud fraction from November
443 through February ranging from ~ 0.25 to ~ 0.40 , while in the summer months (June through
444 September) the low cloud fraction is very small (~ 0.03 - 0.06). The coinciding occurrence of
445 larger fine mode radius values with higher cloud fraction of low altitude clouds from November
446 through February is consistent with the possibility of fog/cloud processing and/or interaction. Of
447 course other factors in addition to cloud processing are also likely to be responsible in part for
448 the larger fine mode radius values in winter such as aerosol humidification at high relative
449 humidity (which is enhanced in the higher RH environment vicinity of clouds), and/or
450 coagulation growth which increases as aerosol concentrations increase (Figure 13b shows
451 somewhat higher AOD in winter months). In Figure 13c the relationship between fine mode
452 radius and aerosol optical depth at 440 nm is shown for the months of November through
453 February only. There is a significant trend of increasing AOD as fine mode radius increases ($r =$
454 0.64), which likely results partly from greater scattering efficiency as particle radius increases, in
455 addition to possibly higher aerosol number concentrations being correlated with larger radius
456 particles.

457

458 **3.4 Additional Sites**

459 Size distributions exhibiting a bimodal accumulation mode have been retrieved at some
460 AERONET sites in eastern China, including Beijing, Xianghe ($\sim 60 \text{ km ESE}$ of Beijing), and
461 Taihu ($\sim 1000 \text{ km SSE}$ of Beijing). Additionally, retrievals with large sub-micron radius that do
462 not show a minimum between the two accumulation modes also occurred at the sites, and they
463 have also been observed at the previously discussed sites. An example from the Beijing site on
464 January 24, 2006 (528 UTC) is shown in Figure 14, where an obvious shoulder in the size

465 distribution suggests a larger submicron mode with radius of $\sim 0.4\text{-}0.5\ \mu\text{m}$, and a smaller fine
466 mode of $\sim 0.20\ \mu\text{m}$ radius, and a total sub-micron radius of the two modes combined at $0.30\ \mu\text{m}$.
467 The aerosol loading for this case was very high, with AOD (440 nm) of 2.87 and $\alpha_{440\text{-}870}$ of 1.04.
468 The retrieved coarse mode (super-micron) AOD was nearly spectrally constant at ~ 0.05 ,
469 therefore the resultant fine mode fraction of AOD was 0.98 at 440 nm and 0.96 at 870 nm. The
470 MODIS Aqua satellite image (not shown) from ~ 1 hour 20 min before this retrieval shows
471 stratiform cloud in the immediate vicinity of the Beijing site and the grayish color of the cloud
472 suggests that there are aerosols above cloud top altitude, thereby suggesting these nearest clouds
473 are at a relatively low altitude. The study of *Niu et al.* [2010] found that the frequencies of fog
474 events in wintertime over eastern-central China have doubled over the past three decades in
475 response to changes in atmospheric circulation. This increase in fog incidence in the region
476 would likely result in increased probability of aerosol modification by fog processing. As
477 previously mentioned, *Li et al.* [2011] made in situ measurements of aerosols under highly
478 polluted conditions from Mt. Tai (~ 1.5 km altitude; ~ 420 km SSE of Beijing) and found that the
479 cloud residue particles (or cloud processed aerosols) had radius of $\sim 0.40\ \mu\text{m}$ (number
480 distribution) that were approximately twice as large as the interstitial aerosols, or aerosols that
481 did not interact with clouds. Also at Anmyon Island on the west coast of South Korea across the
482 Yellow Sea from this region of China, some AERONET retrievals were identified with bimodal
483 sub-micron size distributions, associated with clouds near the site. On one day, November 15,
484 2007, three retrievals within a 2 hour interval showed a decrease in the larger accumulation mode
485 with time, similar to that shown in Figure 12b at Fresno.

486 Additional sites in Asia where AERONET bimodal accumulation mode size distributions
487 retrievals occurred were located in Taiwan and continental Southeast Asia. Three sites in Taiwan
488 (Chen Kung Univ, NCU Taiwan, and Taipei CWB) had some of these size distribution retrievals,
489 suggesting cloud processing of aerosol. On one day, March 3, 2007, two sites near the west coast
490 (within $\sim 5\text{-}15$ km of the ocean), Taipei CWB and Chen-Kung Univ (~ 260 km apart), showed
491 similar bimodal fine mode retrievals (not shown) and the Terra and Aqua MODIS images
492 showed extensive stratiform cloud over the waters of the Taiwan Strait to the west and also
493 stratiform cloud to the east and north over the Pacific on that day. Therefore a large region in and
494 near Taiwan may have been covered with this aerosol type on this date. In Southeast Asia, two
495 sites in Thailand (Silpakorn – near to Bangkok; Chiang Mai Met Sta – in the north) and one in

496 Vietnam (Bac Giang – in the north, near Hanoi) all have had a few cases of bimodal fine mode
497 size distribution retrievals that have occurred in conditions of extensive nearby cloud cover.

498 In Europe, AERONET sites located in the Po Valley and nearby valleys in northern Italy
499 exhibited some retrievals showing bimodal accumulation mode size distributions. The
500 AERONET site names are Ispra, Modena, Venice, and ISDGM_CNR located throughout the Po
501 Valley region with Ispra in the west and Venice in the East (~307 km apart), with the Venice site
502 located on a platform in the Adriatic Sea ~13 km east of Venice. These bimodal fine mode
503 retrievals were also associated with nearby low altitude fog or stratiform cloud (evident from
504 MODIS images), thereby also suggesting cloud processing of the aerosol. An intensive field
505 campaign to study primarily the fog and also the aerosols in this region was conducted in 1989,
506 called ‘The Po Valley Fog Experiment 1989’ [Heintzenburg, 1992; Fuzzi *et al.*, 1992]. During
507 this field campaign, *Svenningsson et al.* [1992] measured the hygroscopic growth of ambient
508 interstitial particles in the fog environment, and found that there were two general modes of
509 accumulation size aerosol with different hygroscopic growth rates, with, on average, equal
510 numbers of particles in each mode. Also from this same field experiment, *Noone et al.* [1992]
511 presented in situ measurements of aerosol size distributions both pre-fog and during the fog
512 events. Their measured volume size distribution radius values of the residual aerosol mode
513 during these fog events peaked from ~0.30 - 0.35 μm , compared to the pre-fog peak radius of
514 ~0.12 μm . These aerosol radii are similar in size (but somewhat smaller) to the AERONET
515 retrieved radius values of ~0.4-0.5 μm for the cloud processed or ‘residual’ mode in this region,
516 and the smaller fine mode retrieved radius is usually larger than 0.12 μm , typically ranging from
517 ~0.15-0.20 μm .

518 Another region in Europe where a few retrievals of bimodal accumulation mode aerosols
519 have been observed is ~40-60 km inland from the North Sea at the Lille site in northern France
520 and at the Cabauw site in the Netherlands. Again, extensive stratiform clouds were apparent in
521 MODIS images at times relatively close to the almucantar times of these ‘cloud processed’
522 aerosol cases.

523 Very few cases of bimodal accumulation mode aerosol retrievals were identified from South
524 American AERONET sites, however measurements made in Sao Paulo, Brazil on July 2, 2007
525 provide a very informative case study. Figure 15a shows the MODIS Terra and Aqua images on
526 this date, with stratiform cloud near the site at the Terra overpass time (1300 UTC) and most of

527 these clouds have evaporated by the time of the Aqua overpass (1720 UTC), except along the
528 coast and over the ocean. There were no direct sun measurements of AOD acquired prior to
529 ~1200 UTC due to cloud cover obscuring the sun. Observations (3 hourly) from the weather
530 station at Sao Paulo airport showed 100% cloud cover at 0300 and 0600 UTC and decreasing to
531 90% and 60% at 0900 and 1200 UTC respectively and no clouds at 1500 UTC. These were
532 clouds with low base altitude, ranging from 150 m at 0300 UTC to 250 m at both 0600 and 0900
533 UTC and 450 m at 12 UTC. Surface relative humidity ranged from 86-89% from 0600-1200
534 UTC, falling to 62% at 1500 UTC and 39% at 1800 UTC. Figure 15b shows time series of the
535 Level 2.0 AOD (500 nm) and $\alpha_{440-870}$ for the complete day of observations with AOD shortly
536 after cloud dissipation of ~0.40 and decreasing to ~0.16 by the end of the day. Angstrom
537 exponent increased throughout the day, beginning at ~0.85 shortly after cloud dissipation and
538 reaching a maximum of ~1.55 at the end of the day. The aerosol volume size distribution
539 retrievals made from ~1300 to ~1900 UTC (7 retrievals) are shown in Figure 15c with all
540 retrievals showing very low residual errors (<3.2%), computed from the comparison of
541 measured to modeled sky radiances. Only the retrievals made at 1412 and 1612 UTC are not
542 designated as Level 2 because the solar zenith angles were less than 50 degrees (both ~49
543 degrees). The sub-micron radius size distributions show very large dynamics over the day during
544 this 6-hour time interval, however the coarse mode size is relatively constant and the computed
545 coarse mode AOD was relatively constant as well, ranging from ~0.011 to 0.015 (also nearly
546 constant in wavelength). Bimodal sub-micron size distributions are evident for 3-4 hours, with
547 the earliest retrieval (1312 UTC) showing the larger mode at ~0.44 μm and the smaller mode at
548 ~0.11 μm . The radius of the smaller mode remains at ~0.11 μm while the larger mode radius
549 decreases to ~0.38 μm at 1412 UTC and then to ~0.34 μm at 1612 UTC. A hint of this larger
550 mode remains at 1712 UTC with a yet further reduced radius. This decrease in magnitude and
551 shift in radius of the larger fine mode particles suggests dissipation and perhaps drying out of
552 these aerosols after cloud dissipation and with RH continuing to decrease throughout the day. It
553 is also possible that some advection of differing aerosol types may have occurred throughout the
554 day, since winds of ~2-3 m/sec blew from the northeast to east during this interval. However
555 these are relatively light horizontal winds so it is expected that much of the size distribution
556 dynamics are likely to have occurred from aerosol interaction with clouds and also hygroscopic
557 growth in the changing RH environment.

558

559 **4. Discussion**

560 The primary focus of this paper is to examine volume size distribution retrievals that exhibit
561 bimodality in the submicron radius size range for cases where stratiform clouds or fog have
562 recently dissipated, thereby strongly suggesting aerosol-cloud interactions and cloud processing
563 of aerosols. However these types of retrievals are quite rare in the AERONET database in part
564 since relatively cloud-free observations of sky radiance angular distributions are required over a
565 large range of scattering angles to enable high quality almucantar retrievals. Also, at the same
566 time, a significant fraction of the total aerosols need to have been modified by interactions within
567 the cloud environment in order for the column integrated size distribution to exhibit a separate
568 size mode. This process may occur when low altitude stratiform cloud and/or fog have vertical
569 distributions that show significant overlap with the aerosol layer, and subsequently the cloud
570 dissipates (evaporates) over a relatively large area. Therefore, although these types of retrievals
571 are very rare (much less than 1% of retrievals), it seems likely that these types of cloud processed
572 aerosols are much more common than would be inferred from the very low frequency of such
573 AERONET observations. If there is only partial dissipation of the cloud or fog, then some sky
574 radiances remain cloud contaminated and the retrieval is not likely to be robust or even possible.
575 Additionally, cloud processing and aerosol-cloud interactions also occur within cumulus type
576 cloud environments and AERONET observations of cloud-processed aerosols for these types of
577 cases are even more challenging to observe from almucantar scans. This is partly due to the
578 previously mentioned cloud contamination issue for broken or scattered cumulus fields that
579 precludes the ability to perform a robust retrieval. The aerosol field also needs to be spatially
580 relatively uniform in order to achieve retrievals with small errors. Additionally, for cumulus
581 cloud fields with less fractional coverage, and therefore more likely yielding a good retrieval
582 (small error between measured and computed sky radiances), the fraction of the aerosol column
583 that interacts with clouds is relatively small and therefore much less likely to exhibit a separate
584 mode in a column integrated aerosol size distribution. Cumulus clouds over land (where most
585 AERONET sites are located) also tend to have base altitudes that are often in the upper portion
586 of the aerosol boundary layer thereby possibly limiting the potential for aerosol-cloud interaction,
587 although vertical convection may offset this with aerosol transport in updrafts into cumulus
588 clouds.

589 An example of a site where very few observations of bimodal sub-micron mode size
590 distribution retrievals have occurred is the Goddard Space Flight Center (GSFC) site in
591 Greenbelt, Maryland in the mid-Atlantic region of the USA. The GSFC site is the AERONET
592 inter-calibration center and the reference Cimel instruments located there are calibrated at Mauna
593 Loa Observatory thereby insuring highly accurate AOD (<0.005 in the visible and near IR; *Eck*
594 *et al.* [1999]). Low altitude stratiform clouds that are coincident in altitude with the aerosol layer
595 and deep vertical extent fog are very rare at this site, although cumulus clouds are very common
596 on days when almucantar retrievals are possible. Nearly continuous AERONET measurements
597 have been made at the GSFC site for over 18 years as of the end of 2010, yet only five days were
598 identified where sub-micron bimodal size distribution retrievals occurred. Retrievals from two of
599 these days are shown in Figure 16, along with a retrieval exhibiting a single mode of very large
600 sub-micron radius. The bimodal cases at GSFC exhibit less of a distinct larger mode (shallower
601 minimum between modes) than most of the cases shown for previous sites and also at a
602 somewhat smaller radius. The larger mode radius for these sub-micron bimodal cases ranged
603 from ~ 0.30 to ~ 0.33 μm . Although smaller than the ~ 0.4 - 0.5 μm range of most of the retrievals
604 presented in this paper, this radius range is also within the size range reported from some in situ
605 measured and model computed cloud or fog processed aerosol sizes. All of these cases had time
606 series of AOD on those dates that suggested significant cloud cover before and/or after the
607 retrievals, due to the lack of AOD measurements available. Additionally, the mono-modal case
608 shown from July 14, 2006 (AOD(440 nm)=0.79) was the retrieval that had the largest computed
609 fine mode volume median radius at the GSFC site, for the subset of data that had columnar water
610 vapor amount (PW) exceeding 3 cm. The peak fine mode radius on this date was 0.37 μm , and
611 there was also much cloud cover in the region as evidenced by both missing AOD for the entire
612 two previous days (all data were cloud screened) and at ~ 30 minutes after this scan was taken in
613 the early morning and other times during the day, and from extensive regional cloud cover in the
614 Terra MODIS image at ~ 4 hours after the retrieval time. The $\alpha_{440-870}$ for this case was 1.20, and
615 the AOD spectra was also very non-linear as parameterized by $\alpha' = 1.79$ (a very high value),
616 therefore consistent with very large fine mode aerosol size. It is noted that two other secondary
617 reference instruments located at GSFC on this date and time retrieved essentially the same size
618 distribution as from the primary reference, shown in Figure 16.

619 The climatological average size distributions as a function of AOD level for the GSFC site
620 are shown in Figure 17. These are a subset of the complete set of Level 2 size distributions when
621 columnar water vapor amount (precipitable water, PW) exceeds 3 cm. This threshold of high
622 water vapor amount effectively excludes cases when smoke has been transported to the GSFC
623 site, sometimes from distant sources as was shown in *Eck et al.* [2003]. Days with high PW are
624 also more likely to have higher relative humidity and cloud cover than days with low PW. The
625 average size distributions at all AOD levels in Figure 17 are dominated by the fine mode, with
626 the fine mode fraction of AOD at 440 nm ranging from 0.89 to 0.99, and computed coarse mode
627 AOD of ~ 0.02 at all wavelengths. The fine mode, shown isolated in Figure 17b, clearly exhibits
628 an increase in radius as AOD increases throughout the measured range of AOD. The average fine
629 mode volume median radius increased steadily from $\sim 0.15 \mu\text{m}$ at $\text{AOD}(440\text{nm}) = 0.15$ to a
630 radius of $0.24 \mu\text{m}$ at $\text{AOD}(440\text{nm}) = 1.55$. Since all of these retrievals were made under high
631 PW conditions it is assumed that the relative humidity did not vary over a very wide range as a
632 function of AOD. Therefore the observed increase in fine mode radius as AOD increased may
633 have largely resulted from aerosol coagulation since coagulation rate increases as concentration
634 increases [*Reid et al.*, 1998]. However humidification may still have been significant in
635 conjunction with cloud interaction or in the high humidity halo surrounding clouds, especially
636 since US mid-Atlantic coast aerosol is strongly hygroscopic [*Kotchenruther et al.*, 1999]. In
637 conjunction with the increase in radius there was also a general trend of increasing average width
638 of the size distribution as AOD increased. An increase in the width of the fine mode distribution
639 that occurred as aerosol concentrations increased may possibly have been caused by mixtures of
640 larger aged aerosols combined with freshly emitted or recently formed smaller particles (from
641 gas to particle conversion). *Thornhill et al.* [2008] analyzed aircraft in situ measurements of
642 volume size distribution for the US east coast and Midwestern region and found significantly
643 larger particles (and greater width) at higher altitude (2-4 km) than from the surface to 2 km,
644 perhaps due to more aging and cloud interaction at higher altitudes. Additionally, at GSFC,
645 aerosol-cloud interactions may have resulted in some increase in the larger tail or shoulder of the
646 fine mode distribution (the $0.3 \mu\text{m}$ radius line is denoted in Figure 17 as a general marker of
647 large and therefore possibly cloud processed accumulation size aerosol). As the AOD increases
648 in the mid-Atlantic region of the US it is highly probable that an increasing fraction of the
649 aerosols are aged from one to several days. *Lelieveld and Heintzenburg* [1992] utilized estimates

650 of cloud fraction and lifetimes to infer that globally the average sulfate particle goes through 3 to
651 7 cloud condensation-evaporation events over its average one-week lifetime before removal from
652 the atmosphere. Although it is beyond the scope of this paper to investigate this possibility, it
653 was suggested by *Jeong and Li* [2010], from analysis of AERONET AOD in conjunction with
654 cloud fraction data at a site in Oklahoma, that the increase of AOD in the vicinity of clouds was
655 likely caused by cloud processing of aerosols more than from aerosol humidification.

656 It is noted that the size distributions in Figure 17 for the GSFC site differ from those
657 presented for the same site in *Dubovik et al.* [2002], hereafter designated D02. This is due to
658 improvements made to the retrievals in Version 2 (V2) versus the pre-Version 1 retrievals used
659 in D02 [see *Eck et al.* 2008 for a brief discussion of V2]. The width (geometric standard
660 deviation) of the fine mode for the GSFC site in D02 is significantly narrower at 1.46 (compared
661 to ~1.51 to 1.60 in V2), and was also constant as a function of AOD. Additionally, the fine mode
662 volume median radius values in D02 differ somewhat from those shown in Figure 17, being
663 smaller at lower AOD and larger at the highest AOD levels than V2. This is not a result of the
664 data shown here being only those retrievals for which $PW > 3$, since very similar values of median
665 radius and width occur when all the Version 2 GSFC retrievals are analyzed, regardless of PW
666 level. The aerosol absorption for the GSFC site is slightly greater in V2 for the data where
667 $AOD(440\text{ nm}) > 0.4$, with average imaginary refractive index at ~0.004 versus ~0.003 in D02.
668 This results in average SSA being 0.01 lower than in D02, at 0.97, 0.96, 0.95, and 0.94 at the
669 wavelengths 440, 675, 870 and 1020 nm, respectively.

670

671 **5. Summary and Conclusions**

672

673 The largest radius fine mode (sub-micron radius) dominated aerosol size distributions
674 retrieved from AERONET almucantar scans have been observed after fog or cloud dissipation
675 events. These types of column-integrated size distributions have been observed at several
676 AERONET sites in many regions of the world after evaporation of low altitude cloud such as
677 stratocumulus or fog (essentially cloud with base at ground level). These cases with ‘cloud
678 processed’ aerosol are sometimes bimodal in the accumulation mode with the large size mode
679 often at ~0.4 – 0.5 μm radius (volume distribution); the smaller mode typically at ~0.12 to ~0.20
680 μm may be interstitial aerosol that were not modified by incorporation in droplets and/or aerosol

681 that are less hygroscopic in nature. The smaller mode may also result from aerosols that were at
682 altitudes above (or below) cloud layers, thereby not interacting with clouds. Bimodal
683 accumulation mode size distributions have often been observed with in situ measurements of
684 aerosols that have interacted with clouds.

685 In situ measurements of ambient aerosols after fog dissipation (e.g. London, England and
686 the San Joaquin Valley, CA) have shown particles in the same or similar size range (modal peak
687 at $\sim 0.4 - 0.5 \mu\text{m}$ volume distribution radius) that are composed of hydroxymethanesulphonate
688 (HMS), which are formed exclusively in the aqueous phase within cloud or fog droplets.

689 Additional in situ measurements of large size aerosol (submicron radius) have also been made in
690 Eastern China, and the Po Valley, Italy associated with cloud processing of aerosol. Therefore
691 AERONET aerosol size distribution retrievals, made after dissipation of cloud and/or fog, are in
692 good agreement with particle sizes measured by in situ techniques for cloud-processed aerosols.

693 The number of AERONET retrievals where a bimodal sub-micron size distribution is
694 observed, including a cloud-processed mode, is a very small percentage of the total retrievals.
695 This is due in part to the requirement of nearly cloudless conditions for the range of angular sky
696 radiances needed for a good retrieval. This is characteristic of the biases of remote sensing
697 measurements of aerosol properties towards conditions of low cloud fraction, both from ground
698 and satellite sensors. Additionally a significant portion of the aerosol layer and cloud/fog layer
699 needs to be coincident in order for the aerosol-cloud interactions to occur over a large enough
700 fraction of the aerosol loading to be able to observe a separate mode in column-integrated size
701 distributions. Since AOD was observed to increase as fine radius increased, the sampling bias of
702 cloud processed aerosols in the near cloud environment likely results in an underestimation of
703 total AOD from most satellite and ground based remote sensing observations, and therefore
704 underestimation of aerosol direct radiative forcing.

705 It is also noted that these types of fine mode bimodal size distributions have only been
706 observed from AERONET retrievals in polluted conditions in regions where sulfate is known to
707 be a significant aerosol species. There have been no cases of bimodal sub-micron size
708 distributions observed in regions and seasons when biomass-burning aerosols dominate, possibly
709 due in part to the less soluble and less hygroscopic nature of biomass burning aerosols and also
710 possibly due to the types of clouds and their relative altitude with respect to the smoke layers in
711 these regions.

712 Aerosols of this type and large size range may also be formed by cloud processing in partly
713 cloudy conditions in lower concentrations and may contribute to the ‘shoulder’ of larger size
714 particles in the accumulation mode retrievals, especially in regions where sulfate or other highly
715 soluble aerosol are a significant component of the total aerosol composition.

Acknowledgements. The AERONET project was supported by Michael D. King, retired in 2008 from the NASA EOS project office, and by Hal B. Maring, Radiation Sciences Program, NASA Headquarters. The IIT Kanpur AERONET site was operational since January 2001 under a joint agreement between IIT Kanpur and NASA. We acknowledge the efforts of Harish Vishwakarama in the operation of this AERONET site. One of the authors, M. Rivas, acknowledges support by UTA-Mayor Grant 4721 (2011-2012).

References

- Albrecht, B.A., Aerosols, cloud microphysics, and fractional cloudiness (1989), *Science*, 245 (4923), 1227-1230.
- Alkezweeny, A.J., Field observations of in-cloud nucleation and the modification of atmospheric aerosol-size distributions after cloud evaporation (1995), *J. Appl. Meteor.*, 34(12), 2649-2654.
- Allen, G. et al., (2011), South East Pacific atmospheric composition and variability sampled along 20° S during VOCALS-Rex, *Atmos. Chem. Phys.*, 11, 5237–5262.
- Badarinath, K. V. S., Shailesh Kumar Kharol, Anu Rani Sharma, and P. S. Roy (2009), Fog Over Indo-Gangetic Plains—A Study Using Multi-satellite Data and Ground Observations, *IEEE J. Selected Topics In Applied Earth Observations And Remote Sensing*, 2 (3), 185-195.
- Baxla, S.P., A.A. Roy, Tarun Gupta, S.N. Tripathi, R. Bandyopadhyaya (2009), Analysis of Diurnal and Seasonal Variation of Submicron Outdoor Aerosol Mass and Size Distribution in a Northern Indian City and Its Correlation to Black Carbon, *Aerosol Air Qual. Res.*, 9, 458-469.
- Bretherton, Christopher S., T. Uttal, C.W. Fairall, S. E. Yuter, R. A. Weller, D. Baumgardner, K. Comstock, R. Wood, G. B. Raga (2004), The Epic 2001 Stratocumulus Study, *Bull. Amer. Meteor. Soc.*, **85**, 967–977, doi: 10.1175/BAMS-85-7-967
- Carn, S. A., A. J. Krueger, N. A. Krotkov, K. Yang, and P. F. Levelt (2007), Sulfur dioxide emissions from Peruvian copper smelters detected by the Ozone Monitoring Instrument, *Geophys. Res. Lett.*, 34, L09801, doi:10.1029/2006GL029020.
- Chand, D., D. A. Hegg, R. Wood, G. E. Shaw, D. Wallace, and D. S. Covert (2010), Source attribution of climatically important aerosol properties measured at Paposo (Chile) during VOCALS, *Atmos. Chem. Phys.*, 10, 10789–10802.
- Chinnam, N., S. Dey, S. N. Tripathi, and M. Sharma (2006), Dust events in Kanpur, northern India: Chemical evidence for source and implications to radiative forcing, *Geophys. Res. Lett.*, 33, L08803, doi:10.1029/2005GL025278.
- Chow, J. C., L. -W. A. Chen, J. G. Watson, D. H. Lowenthal, K. A. Magliano, K. Turkiewicz, and D. E. Lehrman (2006), PM_{2.5} chemical composition and spatiotemporal variability

- during the California Regional PM10/PM2.5 Air Quality Study (CRPAQS), *J. Geophys. Res.*, *111*, D10S04, doi:10.1029/2005JD006457.
- Clarke, A. D. et al. (2002), INDOEX aerosol: A comparison and summary of chemical, microphysical, and optical properties observed from land, ship, and aircraft, *J. Geophys. Res.*, *107*, 8033, doi:10.1029/2001JD000572.
- Colarco, P. R., M. R. Schoeberl, B. G. Doddridge, L. T. Marufu, O. Torres, and E. J. Welton (2004), Transport of smoke from Canadian forest fires to the surface near Washington, D.C.: Injection height, entrainment, and optical properties, *J. Geophys. Res.*, *109*, D06203, doi:10.1029/2003JD004248.
- Dall'Osto, M., R. M. Harrison, H. Coe, and P. Williams (2009), Real-time secondary aerosol formation during a fog event in London, *Atmos. Chem. Phys.*, *9*, 2459–2469.
- Das, S. K., A. Jayaraman, and A. Misra (2008), Fog-induced variations in aerosol optical and physical properties over the Indo-Gangetic Basin and impact to aerosol radiative forcing, *Ann. Geophys.*, *26*, 1345–1354, 2008
- Dey, S., S. N. Tripathi, R. P. Singh, and B. N. Holben (2004), Influence of dust storms on the aerosol optical properties over the Indo-Gangetic basin, *J. Geophys. Res.*, *109*, D20211, doi:10.1029/2004JD004924.
- Dixon, R. W. and H. Aasen (1999), Measurement of hydroxymethanesulfonate in atmospheric Aerosols, *Atmos. Environ.*, *33*, 2023–2029.
- Dubovik, O., and M. D. King (2000), A flexible inversion algorithm for the retrieval of aerosol optical properties from Sun and sky radiance measurements, *J. Geophys. Res.*, *105*, 20,673–20,696.
- Dubovik, O., A. Smirnov, B. N. Holben, M. D. King, Y. J. Kaufman, T. F. Eck, and I. Slutsker (2000), Accuracy assessments of aerosol optical properties retrieved from AERONET Sun and sky-radiance measurements, *J. Geophys. Res.*, *105*, 9791–9806.
- Dubovik, O., B. N. Holben, T. F. Eck, A. Smirnov, Y. J. Kaufman, M. D. King, D. Tanre, and I. Slutsker (2002), Variability of absorption and optical properties of key aerosol types observed in worldwide locations, *J. Atmos. Sci.*, *59*, 590–608.
- Dubovik, O., et al. (2006), Application of spheroid models to account for aerosol particle nonsphericity in remote sensing of desert dust, *J. Geophys. Res.*, *111*, D11208, doi:10.1029/2005JD006619.
- Eck, T. F., B. N. Holben, J. S. Reid, O. Dubovik, A. Smirnov, N. T. O'Neill, I. Slutsker, and S. Kinne (1999), Wavelength dependence of the optical depth of biomass burning, urban, and desert dust aerosols, *J. Geophys. Res.*, *104*(D24), 31,333–31,349.
- Eck, T. F., B. N. Holben, D. E. Ward, O. Dubovik, J. S. Reid, A. Smirnov, M. M. Mukelabai, N. C. Hsu, N. T. O'Neill, and I. Slutsker (2001), Characterization of the optical properties of biomass burning aerosols in Zambia during the 1997 ZIBBEE Field Campaign, *J. Geophys. Res.*, *106*, 3425–3448.

- Eck, T. F., B. N. Holben, J. S. Reid, N. T. O'Neill, J. S. Schafer, O. Dubovik, A. Smirnov, M. A. Yamasoe, and P. Artaxo (2003), High aerosol optical depth biomass burning events: A comparison of optical properties for different source regions, *Geophys. Res. Lett.*, 30(20), 2035, doi:10.1029/2003GL017861.
- Eck, T. F., et al. (2008), Spatial and temporal variability of column-integrated aerosol optical properties in the southern Arabian Gulf and United Arab Emirates in summer, *J. Geophys. Res.*, 113, D01204, doi:10.1029/2007JD008944.
- Eck, T. F. et al. (2010), Climatological aspects of the optical properties of fine/coarse mode aerosol mixtures, *J. Geophys. Res.*, 115, D19205, doi:10.1029/2010JD014002.
- Fahey, K.M., S.N. Pandis, J.L. Collett Jr., and P. Herckes (2005), The influence of size-dependent droplet composition on pollutant processing by fogs, *Atmos. Environ.*, 39, 4561–4574.
- Fuzzi, S., Facchini, M. C., Orsi, G., Lind, J. A., Wobrock, W., Kessel, M., Maser, R., Jaeschke, W., Enderle, K. H., Arends, B. G., Berner, A., Solly, I., Kruisz, C., Reischl, G., Pahl, S., Kaminski, U., Winkler, P., Ogren, J. A., Noone, K. J., Hallberg, A., Fierlinger-Oberlinninger, H., Puxbaum, H., Marzorati, A., Hansson, H.-C., Wiedensohler, A., Svenningsson, I. B., Martinsson, B. G., Schell, D. And Georgii, H. W. (1992), The Po Valley Fog Experiment 1989. *Tellus B*, 44: 448–468. doi: 10.1034/j.1600-0889.1992.t01-4-00002.x
- Gautam, R., N. C. Hsu, M. Kafatos, and S.-C. Tsay (2007), Influences of winter haze on fog/low cloud over the Indo-Gangetic plains, *J. Geophys. Res.*, 112, D05207, doi:10.1029/2005JD007036.
- Gautam, R., Z. Liu, R. P. Singh, and N. C. Hsu (2009), Two contrasting dust-dominant periods over India observed from MODIS and CALIPSO data, *Geophys. Res. Lett.*, 36, L06813, doi:10.1029/2008GL036967.
- Hansen, J., M. Sato, and R. Ruedy (1997), Radiative forcing and climate response, *J. Geophys. Res.*, 102(D6), 6831-6864.
- Haywood, J., and O. Boucher (2000), Estimates of the direct and indirect radiative forcing due to tropospheric aerosols: A review, *Rev. Geophys.*, 38(4), 513-543.
- Hegg, D. A., D. S. Covert, H. Jonsson, D. Khelif and C. A. Friehe (2004), Observations of the impact of cloud processing on aerosol light-scattering efficiency, *Tellus*, 56B, 285–293
- Heintzenberg, J. (1992), The Po Valley Fog Experiment 1989 What have we learned, where do we go from here?, *Tellus B*, 44: 443–447. doi: 10.1034/j.1600-0889.1991.t01-3-00002.x-il
- Herckes, P., H. Chang, T. Lee, J. L. Collett Jr. (2007), Air Pollution Processing by Radiation Fogs, *Water Air Soil Pollut.*, 181, 65–75, doi 10.1007/s11270-006-9276-x
- Holben, B. N., et al. (1998), AERONET—A federated instrument network and data archive for

- aerosol characterization, *Remote Sens. Environ.*, 66, 1–16.
- Holben, B. N., T. F. Eck, I. Slutsker, A. Smirnov, A. Sinyuk, J. Schafer, D. Giles, and O. Dubovik (2006), AERONET's version 2.0 quality assurance criteria, Remote Sensing of Atmosphere and Clouds, *Proc. SPIE Int. Soc. Opt. Eng.*, 6408, 64080Q, doi:10.1117/12.706524.
- Hoppel, W., G. Frick, J. Fitzgerald, and R. Larson (1994), Marine boundary layer measurements of new particle formation and the effects nonprecipitating clouds have on aerosol size distribution, *J. Geophys. Res.*, 99(D7), 14443-14459.
- IPCC, (2007), Climate Change 2007: The Physical Science Basis, Contribution of Working Group I to the Fourth Assessment Report of the Intergovernmental Panel on Climate Change, Solomon, S., D. Qin, M. Manning, Z. Chen, M. Marquis, K.B. Averyt, M. Tignor and H.L. Miller (eds.), Cambridge University Press, Cambridge, United Kingdom and New York, NY, USA, 996 pp.
- Klein, S. A. and D. L. Hartmann (1993), The Seasonal Cycle of Low Stratiform Clouds. *J. Climate*, 6, 1587–1606. doi: 10.1175/1520-0442(1993)006<1587:TSCOLS>2.0.CO;2
- Koren, I., Y.J. Kaufman, L.A. Remer, and J.V. Martins (2004), Measurement of the Effect of Amazon Smoke on Inhibition of Cloud Formation, *Science*, 303, 5662, 1342-1345, DOI: 10.1126/science.1089424
- Kotchenruther, R., P. Hobbs, and D. Hegg (1999), Humidification factors for atmospheric aerosols off the mid-Atlantic coast of the United States, *J. Geophys. Res.*, 104(D2), 2239-2251.
- Kuang, Z., and Y. L. Yung (2000), Reflectivity variations off the Peru Coast: Evidence for indirect effect of anthropogenic sulfate aerosols on clouds, *Geophys. Res. Lett.*, 27(16), 2501-2504.
- Jacob, D.J., E.W. Gottlieb, and M.J. Prather, 1989. Chemistry of a polluted cloudy boundary layer, *J. Geophys. Res.*, 94 (D10), 12975–13002.
- Jenamani, R. K., Alarming rise in fog and pollution causing a fall in maximum temperature over Delhi (2007), *Current Sci.*, 93(3), 314-322.
- Jeong, M.-J. and Z. Li (2010), Separating real and apparent effects of cloud, humidity, and dynamics on aerosol optical thickness near cloud edges, *J. Geophys. Res.*, 115, D00K32, doi:10.1029/2009JD013547.
- Johnson BT, Osborne SR. 2011. Physical and optical properties of mineral dust aerosol measured by aircraft during the GERBILS campaign. *Q. J. R. Meteorol. Soc.* DOI:10.1002/qj.777
- Lelieveld, J. and J. Heintzenberg (1992), Sulfate Cooling Effect on Climate Through In-Cloud Oxidation of Anthropogenic SO₂, *Science*, 258, 117-120.

- Lewis, J., R. De Young, R. Ferrare, D. A. Chu (2010), Comparison of summer and winter California central valley aerosol distributions from lidar and MODIS measurements, *Atmos. Environ.*, **44**, 4510-4520.
- Li, W., P. Li, G. Sun, S. Zhou, Q. Yuan, W. Wang Cloud residues and interstitial aerosols from non-precipitating clouds over an industrial and urban area in northern China (2011), *Atmospheric Environment* **45**, 2488-2495.
- Lu, M.-L., Jian W., R. C. Flagan, J. H. Seinfeld, A. Freedman, R. A. McClatchey, H. H. Jonsson (2003), Analysis of Humidity Halos around Trade Wind Cumulus Clouds. *J. Atmos. Sci.*, **60**, 1041–1059.
- Munger, J. W., C. Tiller, M. R. Hoffmann (1986), Identification of Hydroxymethanesulfonate in Fog Water, *Science*, **231**, 247-249.
- Niu, F., Z. Li, C. Li, K.-H. Lee, and M. Wang (2010), Increase of wintertime fog in China: Potential impacts of weakening of the Eastern Asian monsoon circulation and increasing aerosol loading, *J. Geophys. Res.*, **115**, D00K20, doi:10.1029/2009JD013484.
- Noone, K. J., Ogren, J. A., Hallberg, A., Heintzenberg, J., Ström, J., Hansson, H.-C., Svenningsson, B., Wiedensohler, A., Fuzzi, S., Facchini, M. C., Arends, B. G. And Berner, A. (1992), Changes in aerosol size- and phase distributions due to physical and chemical processes in fog. *Tellus B*, **44**: 489–504. doi: 10.1034/j.1600-0889.1992.t01-4-00004.x
- Novakov, T., M. O. Andreae, R. Gabriel, T. W. Kirchstetter, O. L. Mayol-Bracero, and V. Ramanathan (2000), Origin of carbonaceous aerosols over the tropical Indian Ocean: Biomass burning or fossil fuels?, *Geophys. Res. Lett.*, **27**(24), 4061–4064.
- Platnick, S., M. D. King, S. A. Ackerman, W. P. Menzel, B. A. Baum, J. C. Riédi, and R. A. Frey (2003), The MODIS Cloud Products: Algorithms and Examples From Terra, *IEEE Trans. Geosci. Remote Sens.*, **41** (2), 459-473.
- Prasad, A. K., R. P. Singh, and M. Kafatos (2006), Influence of coal based thermal power plants on aerosol optical properties in the Indo-Gangetic basin, *Geophys. Res. Lett.*, **33**, L05805, doi:10.1029/2005GL023801.
- Prasad, A. K. and R. P. Singh (2007), Changes in aerosol parameters during major dust storm events (2001–2005) over the Indo-Gangetic Plains using AERONET and MODIS data, *J. Geophys. Res.*, **112**, D09208, doi:10.1029/2006JD007778.
- Pueschel, R. F., P. B. Russell, D. A. Allen, G. V. Ferry, K. G. Snetsinger, J. M. Livingston, and S. Verma (1994), Physical and optical properties of the Pinatubo volcanic aerosol: Aircraft observations with impactors and a Sun-tracking photometer, *J. Geophys. Res.*, **99**(D6), 12,915–12,922.
- Radke, L. F. and P. V. Hobbs, 1991: Humidity and Particle Fields Around Some Small Cumulus Clouds. *J. Atmos. Sci.*, **48**, 1190–1193, doi: 10.1175/1520-

0469(1991)048<1190:HAPFAS>2.0.CO;2

- Rao, X. and Collett Jr., J.L. (1995), Behavior of S(IV) and formaldehyde in a chemically heterogeneous cloud, *Environmental Sci. Tech.*, 29 (4), 1023–1031.
- Reid, J., P. Hobbs, R. Ferek, D. Blake, J. Martins, M. Dunlap, and C. Liousse (1998), Physical, chemical, and optical properties of regional hazes dominated by smoke in Brazil, *J. Geophys. Res.*, 103(D24), 32059-32080.
- Reid, J. S., T. F. Eck, S. A. Christopher, P. V. Hobbs, and B. N. Holben (1999), Use of the Angstrom exponent to estimate the variability of optical and physical properties of aging smoke particles in Brazil, *J. Geophys. Res.*, 104, 27,473– 27,489.
- Reid, J. S., R. Koppmann, T. Eck, and D. Eleuterio (2005), A review of biomass burning emissions part II: Intensive physical properties of biomass burning particles, *Atmos. Chem. Phys.*, 5, 799–825, SRef-ID: 1680-7324/acp/2005-5-799.
- Reid, J. S., B. Brooks, K. K. Crahan, D. A. Hegg, T. F. Eck, N. O'Neill, G. de Leeuw, E. A. Reid, and K. D. Anderson (2006), Reconciliation of coarse mode sea-salt aerosol particle size measurements and parameterizations at a subtropical ocean receptor site, *J. Geophys. Res.*, 111, D02202, doi:10.1029/2005JD006200.
- Reid, J. S., E. A. Reid, A. Walker, S. Piketh, S. Cliff, A. Al Mandoos, S.-C. Tsay, and T. F. Eck (2008), Dynamics of southwest Asian dust particle size characteristics with implications for global dust research, *J. Geophys. Res.*, 113, D14212, doi:10.1029/2007JD009752.
- Schmid, B., J. Michalsky, R. Halthore, M. Beauharnois, L. Harrison, J. Livingston, P. Russell, B. Holben, T. Eck, and A. Smirnov (1999), Comparison of aerosol optical depth from four solar radiometers during the fall 1997 ARM intensive observation period, *Geophys. Res. Lett.*, 26, 2725– 2728.
- Singh, R. P., S. Dey, S. N. Tripathi, V. Tare, and B. Holben (2004), Variability of aerosol parameters over Kanpur, northern India, *J. Geophys. Res.*, 109, D23206, doi:10.1029/2004JD004966.
- Smirnov, A., B. N. Holben, T. F. Eck, O. Dubovik, and I. Slutsker (2000), Cloud screening and quality control algorithms for the AERONET data base, *Remote Sens. Environ.*, 73, 337– 349.
- Su, W., G. L. Schuster, N. G. Loeb, R. R. Rogers, R. A. Ferrare, C. A. Hostetler, J. W. Hair, and M. D. Obland (2008), Aerosol and cloud interaction observed from high spectral resolution lidar data, *J. Geophys. Res.*, 113, D24202, doi:10.1029/2008JD010588.
- Svenningsson, I. B., Hansson, H.-C., Wiedensohler, A., Ogren, J. A., Noone, K. J. And Hallberg, A. (1992), Hygroscopic growth of aerosol particles in the Po Valley. *Tellus B*, 44: 556–569. doi: 10.1034/j.1600-0889.1992.t01-1-00009.x

- Tackett, J. L. and L. Di Girolamo (2009), Enhanced aerosol backscatter adjacent to tropical trade wind clouds revealed by satellite-based lidar, *Geophys. Res. Lett.*, *36*, L14804, doi:10.1029/2009GL039264.
- Tare, V. et al. (2006), Measurements of atmospheric parameters during Indian Space Research Organization Geosphere Biosphere Program Land Campaign II at a typical location in the Ganga Basin: 2. Chemical properties, *J. Geophys. Res.*, *111*, D23210, doi:10.1029/2006JD007279.
- Thornhill, K. L. et al. (2008), The impact of local sources and long-range transport on aerosol properties over the northeast U.S. region during INTEX-NA, *J. Geophys. Res.*, *113*, D08201, doi:10.1029/2007JD008666.
- Tripathi, S. N. et al. (2006), Measurements of atmospheric parameters during Indian Space Research Organization Geosphere Biosphere Programme Land Campaign II at a typical location in the Ganga basin: 1. Physical and optical properties, *J. Geophys. Res.*, *111*, D23209, doi:10.1029/2006JD007278.
- Twohy, C. H., J. A. Coakley, and W. R. Tahnk (2009), Effect of changes in relative humidity on aerosol scattering near clouds, *J. Geophys. Res.*, *114*, D05205, doi:10.1029/2008JD010991.
- Twomey, S., (1977), The Influence of Pollution on the Shortwave Albedo of Clouds. *J. Atmos. Sci.*, *34*, 1149–1152. doi: 10.1175/1520-0469(1977)034<1149:TIOPOT>2.0.CO;2
- Várnai, T. and A. Marshak (2011), Global CALIPSO Observations of Aerosol Changes Near Clouds, *IEEE Geosci. Remote Sens. Lett.*, *8*(1), 19-23.
- Venkataraman, C., G. Habib, A. Eiguren-Fernandez, A. H. Miguel, and S. K. Friedlander (2005), Residential Biofuels in South Asia: Carbonaceous Aerosol Emissions and Climate, *Sci.*, *307*, 5714, 1454-1456.
- Whiteaker, J. R. and K. A. Prather (2003) Hydroxymethanesulfonate as a tracer for fog processing of individual aerosol particles, *Atmos. Environ.*, *37*, 1033–1043.
- Zhang, Q. and X. Ti (2011), High solubility of SO₂: evidence in an intensive fog event measured in the NCP region, China, *Atmos. Chem. Phys. Discuss.*, *11*, 2931–2947, 2011, doi:10.5194/acpd-11-2931-2011.

Figure Captions

Figure 1. Spectral fine mode fraction of AOD (from the Dubovik algorithm almucantar retrievals) versus Angstrom Exponent (440-870 nm) at Kanpur, India for the years 2002-2006 (from Eck et al., 2010). Circled are the outlier values of relatively low Angstrom Exponent (<1.0) and high fine mode fraction (>0.90 at 440 nm) that were all observed during the month of January.

Figure 2. MODIS satellite images centered on the Kanpur, India site (blue circles) from January 5, 2006 [NASA/GSFC Rapid Response]. The morning (515 UTC) Terra image shows fog/cloud adjacent and to the north of Kanpur and the afternoon (~820 UTC) Aqua image shows only haze in the vicinity of Kanpur, with fog having dissipated except in the northern Indo-Gangetic Plain bordering Nepal.

Figure 3. Almucantar retrievals of the aerosol volume size distribution at Kanpur on January 5, 2006 at 837 UTC (only 17 min after the Aqua MODIS image in Figure 2) and at 1006 UTC. Note the bimodality of the sub-micron radius mode.

Figure 4. In situ measured ambient aerosol sizes associated with a fog event in London, (from *Dall'Osto et al.*, [2009] with additional conversion to volume distribution). These large sub-micron particles are composed of hydroxymethanesulphonate (HMS), which is a chemical species that is only formed in aqueous phase chemistry and therefore a tracer for aerosol processing by cloud or fog.

Figure 5. Almucantar retrievals of aerosol single scattering albedo (440 and 675 nm) versus fine mode volume median radius (in microns) at Kanpur, India for January data only, for the interval 2002-2006.

Figure 6. The product of low cloud fraction (cloud top pressure > 600 mb) times low cloud optical depth from the MODIS cloud algorithm [*Platnick et al.*, 2003] at the Terra satellite overpass time (mid-morning) versus the retrieved fine mode median radius (for January 2003 and 2006 only). The retrieved radius values are from almucantar scans made after the fog/low cloud had dissipated, and are daily averages of all retrievals made in a given day.

Figure 7. Almucantar retrieval made at Arica, Chile on July 13, 2008 after the dissipation of the stratocumulus layer over the site. The 440 nm AOD during the almucantar scan averaged 0.58 and the $\alpha_{440-870}$ was 0.77. Similar to the size distribution retrievals at Kanpur (from Figure 3), Figure 7 shows a bimodal submicron size distribution at Arica with the largest of the two modes having a volume radius peak of ~0.48 μm .

Figure 8. (a) The relationship between the almucantar retrieved volume median radius of the fine mode and the magnitude of α' computed from the 380 nm through 870 nm AOD measurements for all Arica retrievals made from 1998-2008. A zero value of α' means that there is no curvature and that the spectral AOD follow the linear or Angstrom relationship in \ln AOD versus $\ln \lambda$. Positive values occur for fine mode dominated size distributions, with α' increasing as accumulation mode radius increases. (b) The relationship between the aerosol optical depth and retrieved fine modal radius at Arica. There is an increasing trend of AOD at 440 nm as fine mode radius increases, with correlation coefficient (r) of 0.48.

Figure 9. The annual variation in the retrieved volume median radius and the low cloud fraction (> 600 mb cloud top pressure) retrieved from the MODIS cloud algorithm with Terra satellite measurements. The MODIS cloud fraction is for a 1 by 1 degree latitude-longitude grid average over the ocean directly to the west of Arica. All individual AERONET retrievals of

fine mode radius from 1998-2008 are shown and the monthly mean low cloud fractions computed from 2001-2009 data are depicted.

Figure 10. (a) Time series of the AERONET measured monthly mean AOD (500 nm) at Arica, Chile from 1998 to 2010, with a gap in the data from April 2004 through May 2007. (b) The daily average SO₂ mass column amounts measured by the OMI satellite instrument [*Carn et al.*, 2007] from September 2004 through 2010. Note that the highest total column SO₂ measured in 2006 through spring 2007, were due to the additional source of the Ubinas volcano eruptions upwind of Ilo.

Figure 11. MODIS Aqua image from Jan 13, 2004 at 2110 UTC showing extensive fog in the Central Valley of California, and the location of Fresno is indicated [NASA/GSFC Rapid Response].

Figure 12. (a) The almucantar size distribution retrieval made at 2332 UTC (75° solar zenith) on January 13, 2004 at Fresno, from approximately 2.4 hours after the MODIS image shown in Figure 11. (b) Size distribution retrievals from Fresno on the morning of February 11, 2006 over a time interval of ~3 hours for these 5 almucantar scans.

Figure 13. (a) All of the individual AERONET retrievals of fine mode radius made at Fresno versus day of the year, for the time interval of 2002-2009. The majority of retrievals with fine mode median radius > 0.20 μm occurred from November through mid-March. Also shown in this figure is the monthly mean low cloud fraction from Terra MODIS (cloud top > 600 mb), averaged over the 2001 through 2009 interval. (b) AOD (440 nm) associated with all of the almucantar retrievals shown in Figure 13a. (c) The relationship between fine mode radius and aerosol optical depth at 440 nm at Fresno is shown for retrievals made during the months of November through February only.

Figure 14. The AERONET size distribution retrieval at the Beijing, China site on January 24, 2006 at 528 UTC, with an obvious shoulder in the size distribution suggesting a larger submicron mode with radius of ~0.4-0.5 μm, with a smaller fine mode of ~0.20 μm.

Figure 15. (a) The MODIS Terra and Aqua images centered on the Sao Paulo, Brazil site (blue circles) on July 2, 2007, with stratiform cloud near the site at the Terra overpass time (1300 UTC) while most of these clouds have evaporated by the time of the Aqua overpass (1720 UTC), except along the coast and over the ocean [NASA/GSFC Rapid Response]. (b) The time series of the Level 2.0 AOD (500 nm) and $\alpha_{440-870}$ for the complete day of observations on July 2, 2007, the date of the MODIS images shown in Figure 15 a. (c) The aerosol volume size distribution retrievals made at Sao Paulo from ~1300 to ~1900 UTC (7 retrievals) on the same date.

Figure 16. Retrievals from the GSFC, Maryland, USA site for two days with bimodal submicron size distributions, along with a retrieval exhibiting a single mode of very large sub-micron radius.

Figure 17. (a) The climatological average size distributions at the GSFC site from 1997-2009, as a function of 440 nm AOD. These are a subset of the complete set of Level 2 size distributions where columnar water vapor amount (precipitable water, PW) exceeds 3 cm. (b) Enlargement of the fine mode only from Figure 17a.

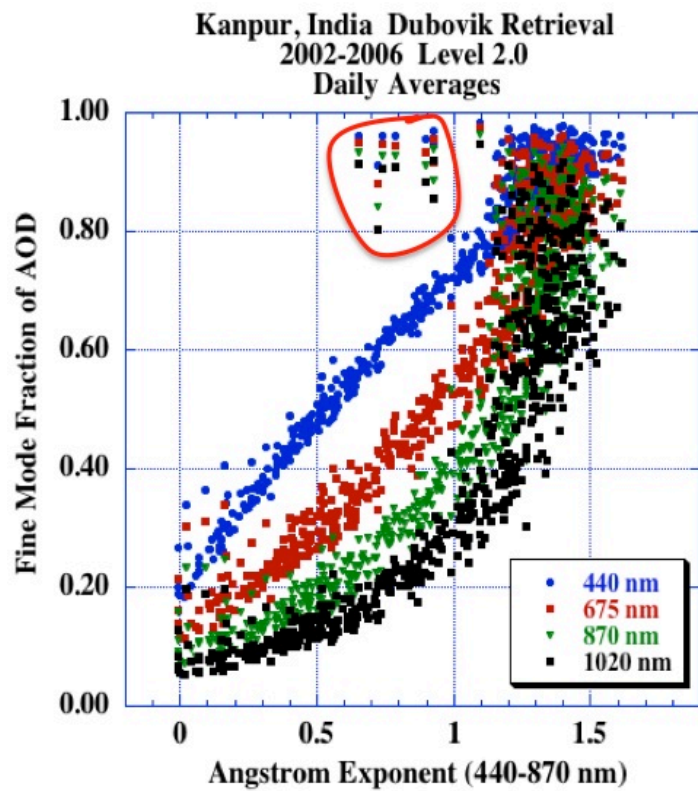


Figure 1.

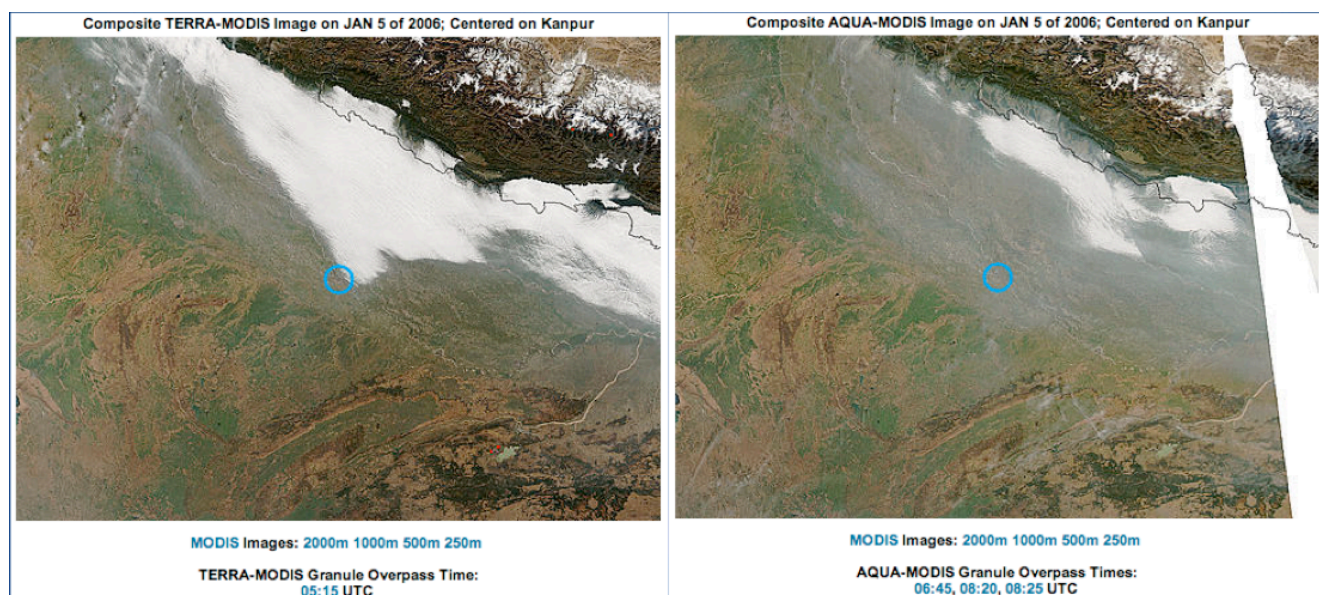


Figure 2.

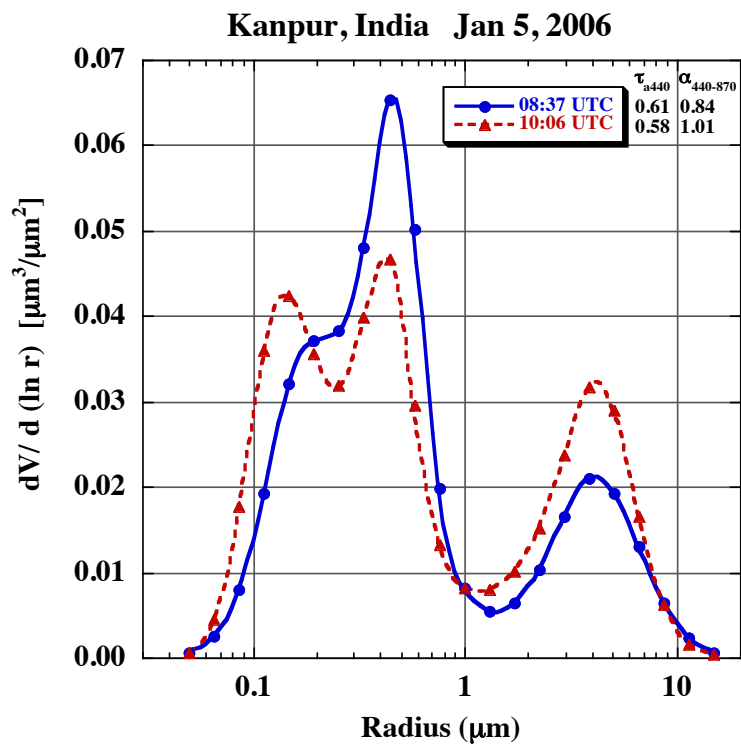


Figure 3.

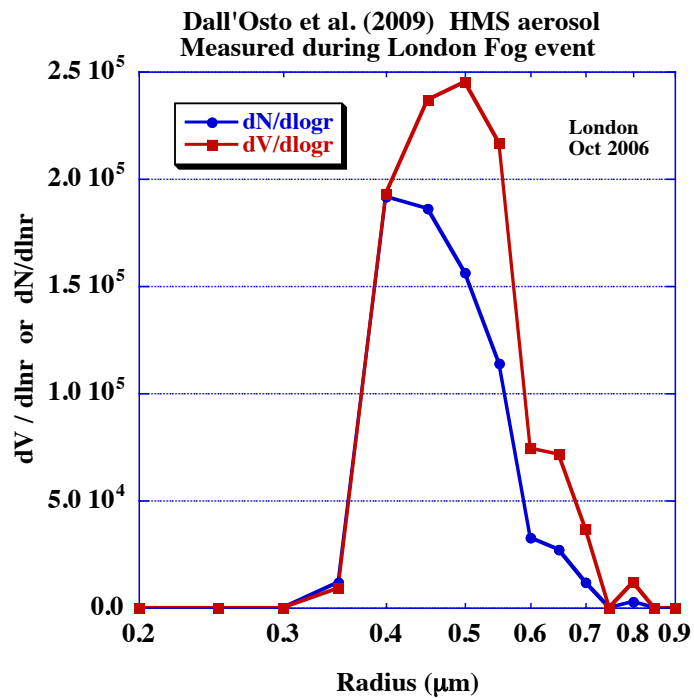


Figure 4.

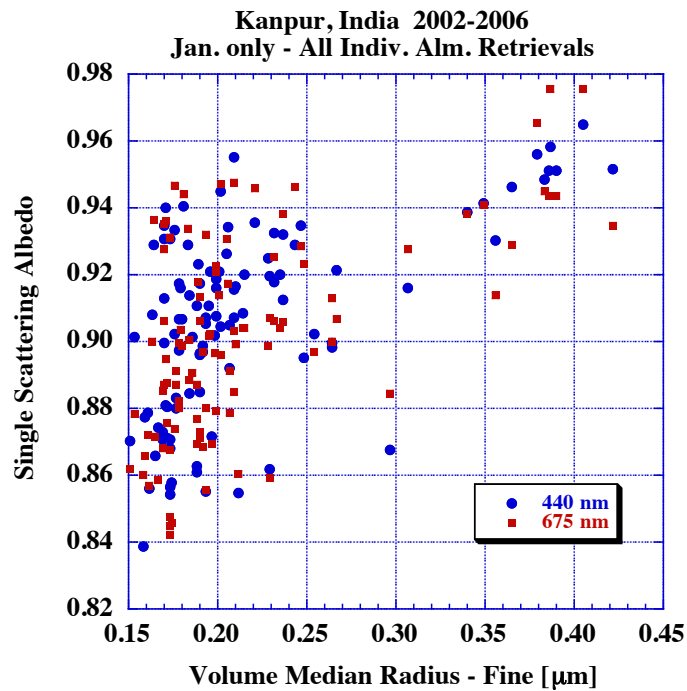


Figure 5.

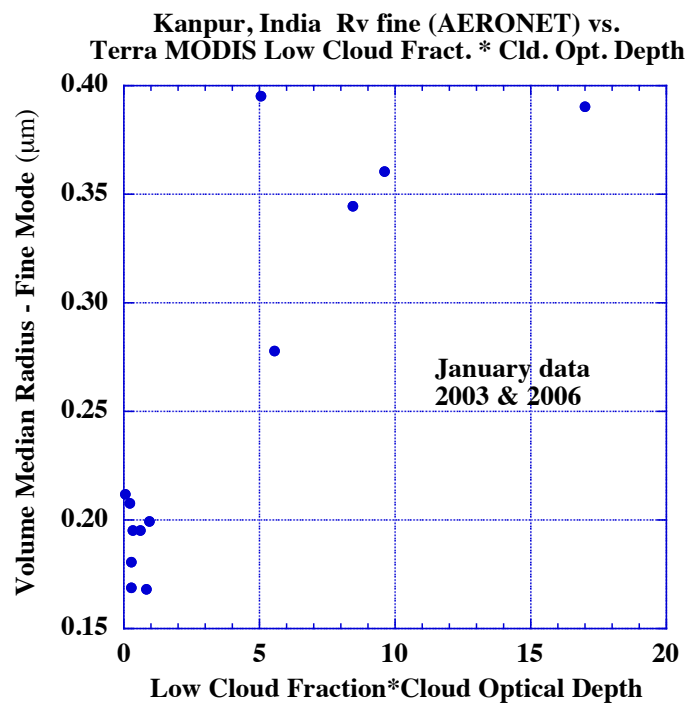


Figure 6.

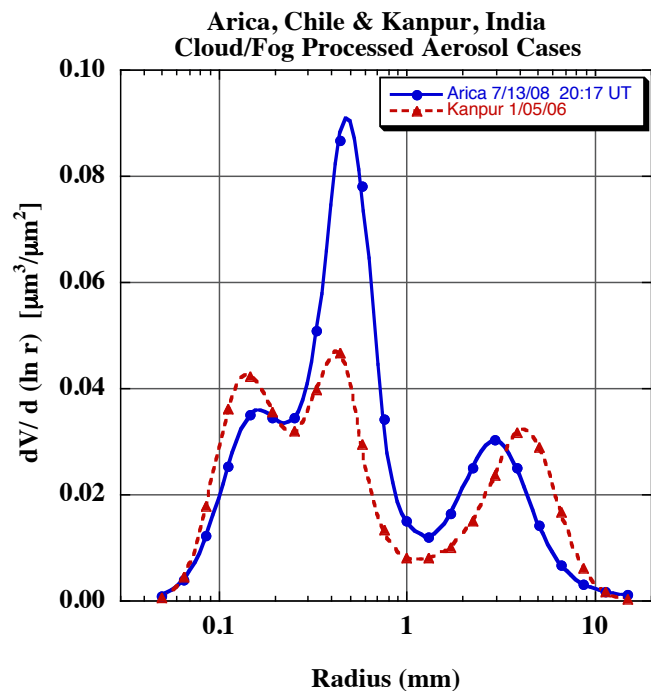


Figure 7.

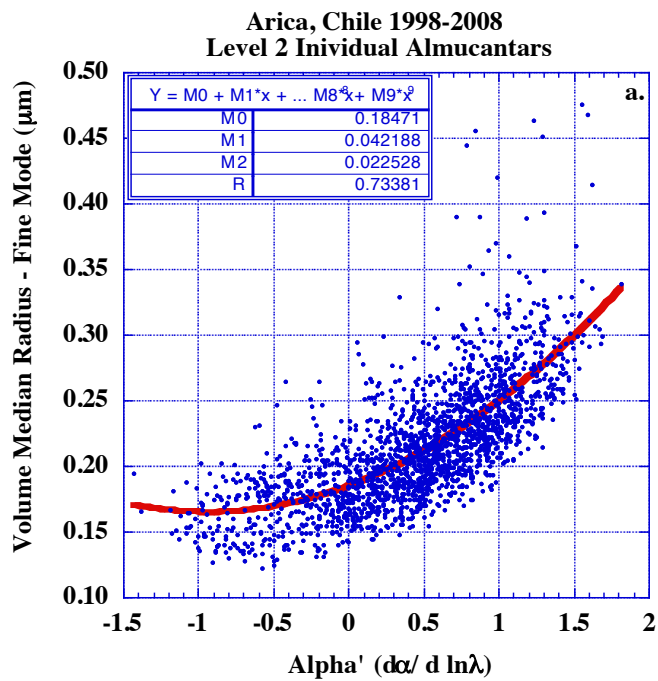


Figure 8a.

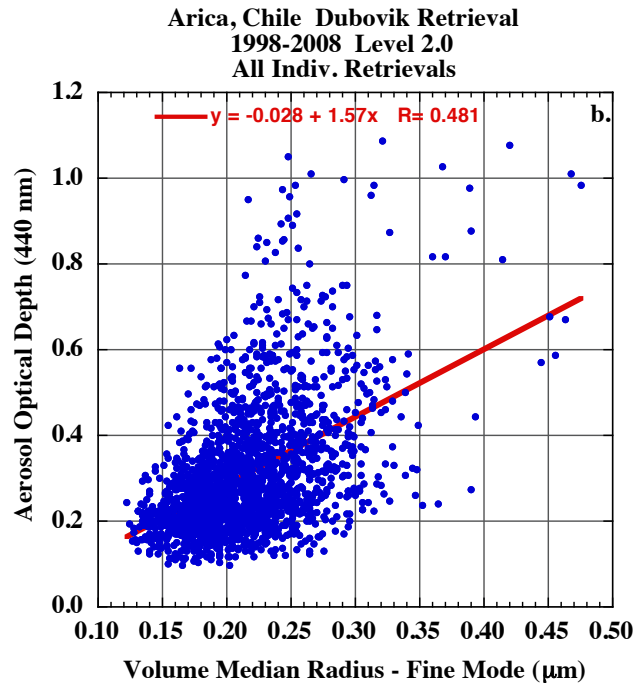


Figure 8b.

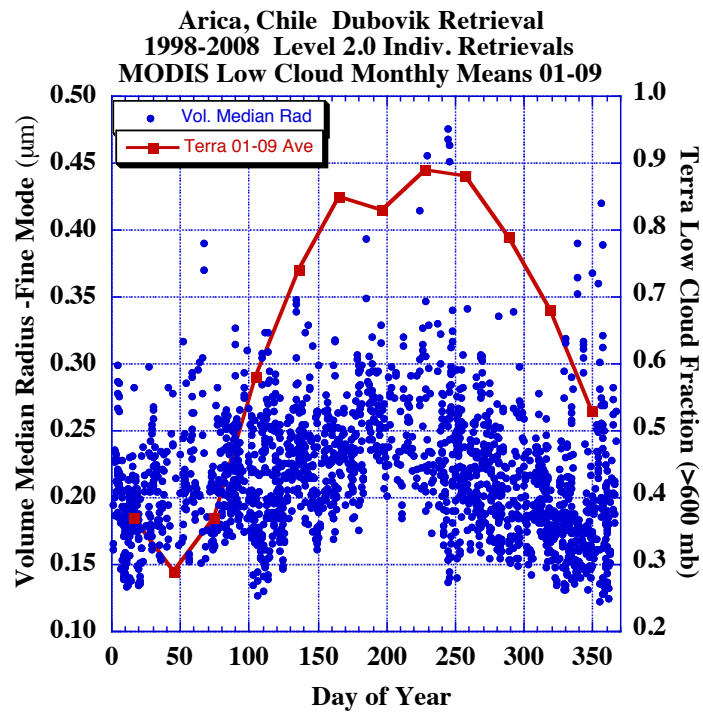


Figure 9.

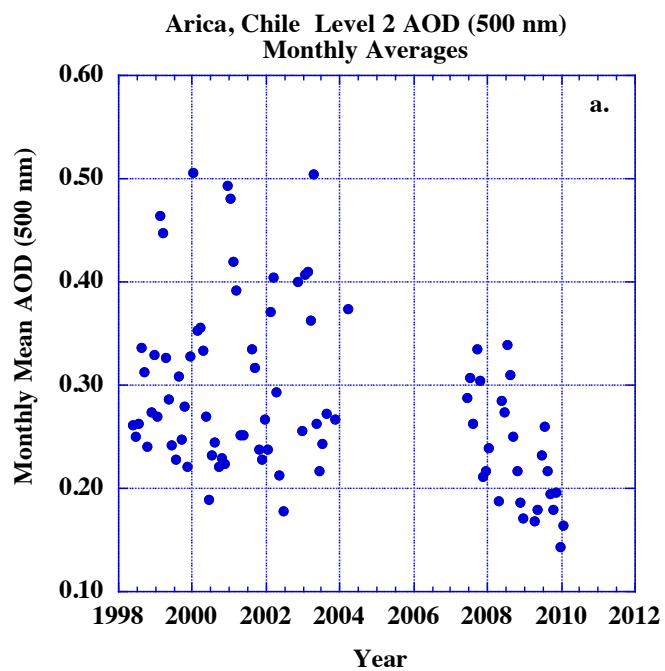


Figure 10a.

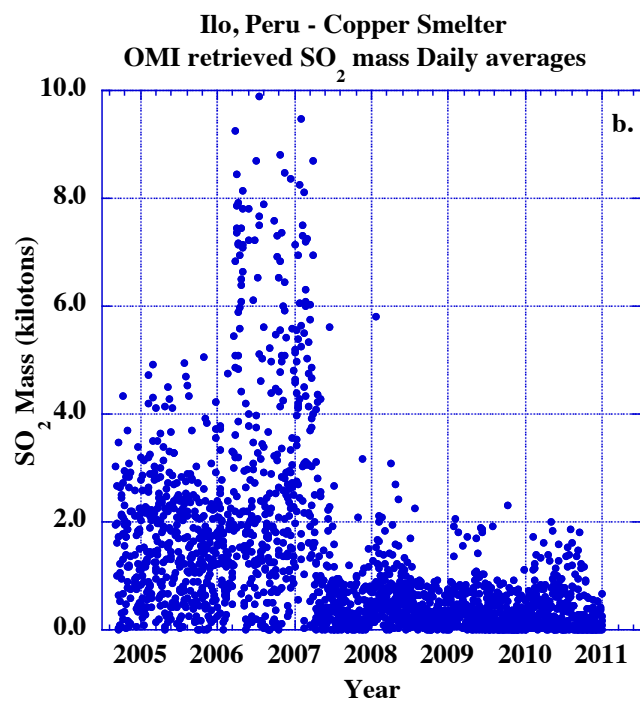


Figure 10b.

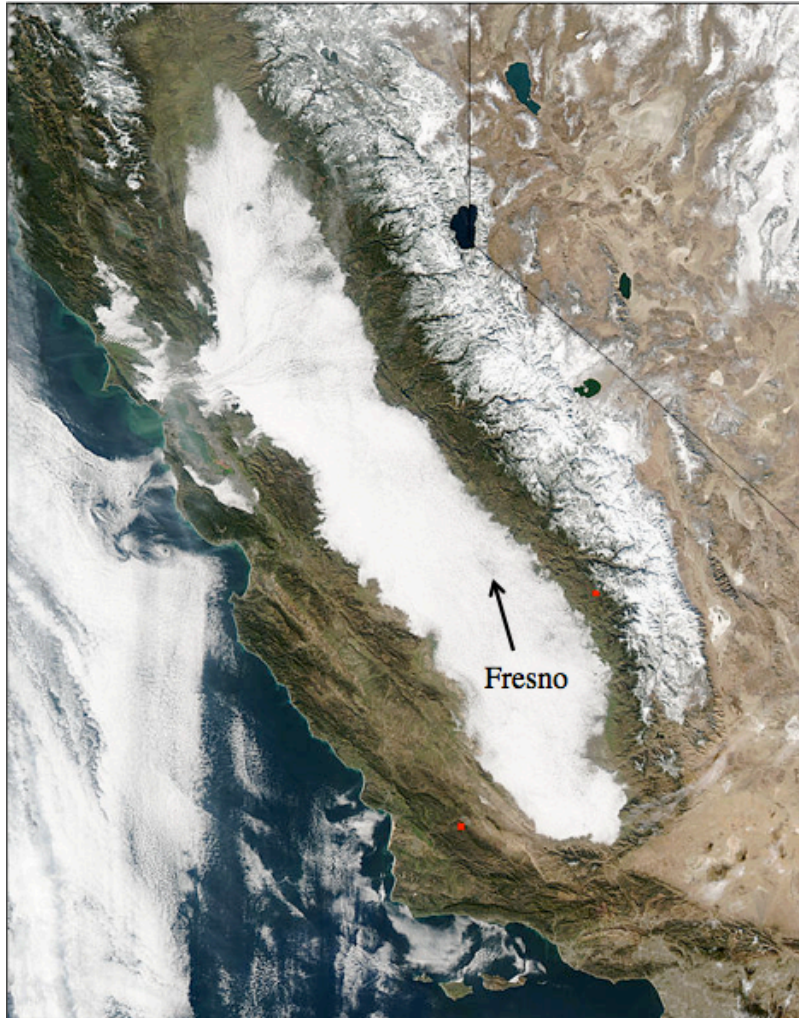


Figure 11. MODIS Aqua image from Jan 13, 2004 at 2110 UTC showing extensive fog in the Central Valley of California.

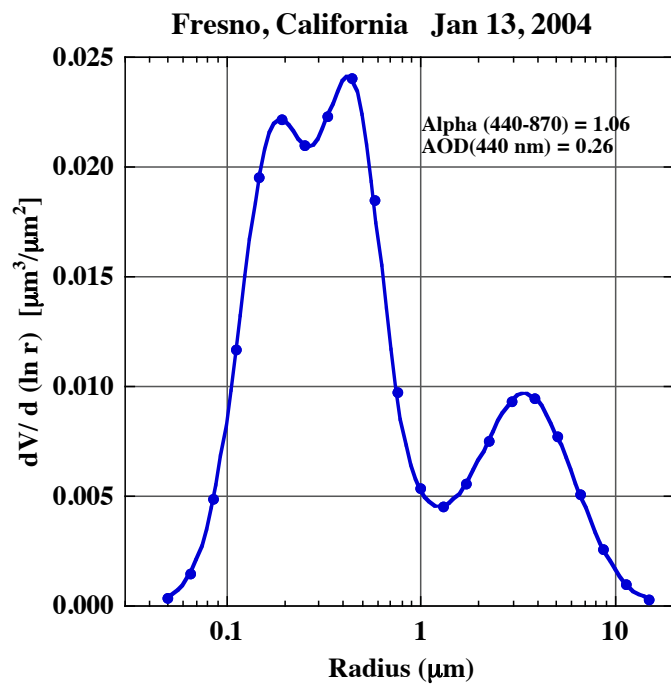


Figure 12a.

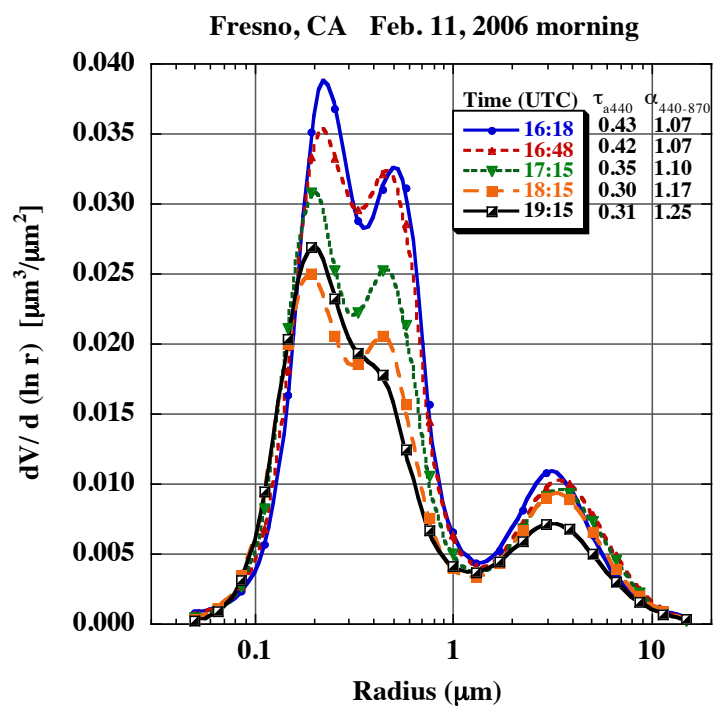


Figure 12b.

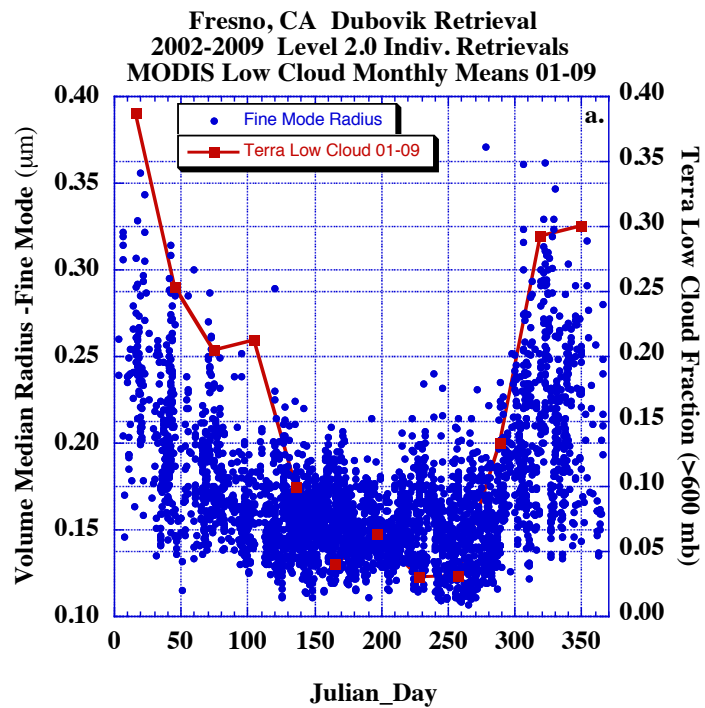


Figure 13a.

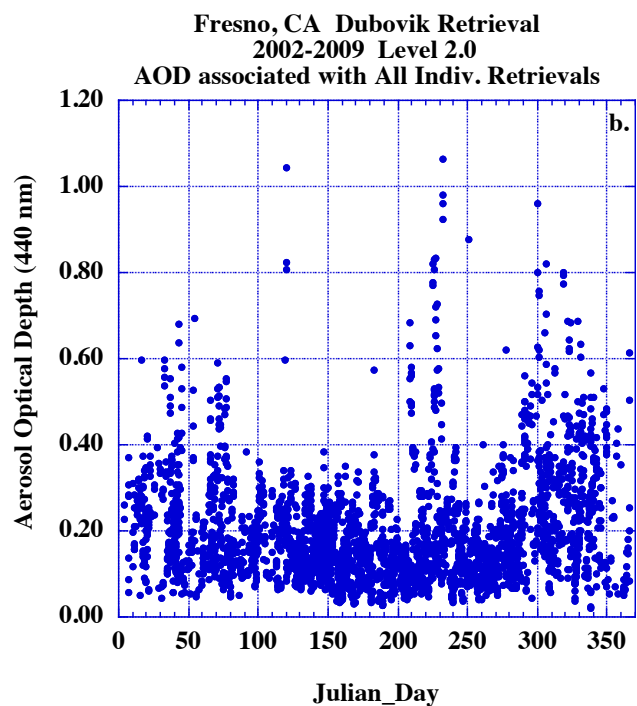


Figure 13b.

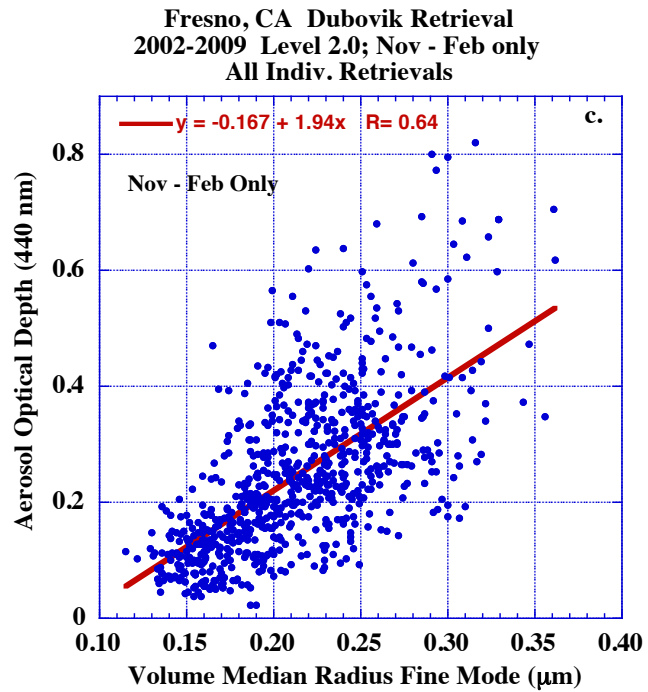


Figure 13c.

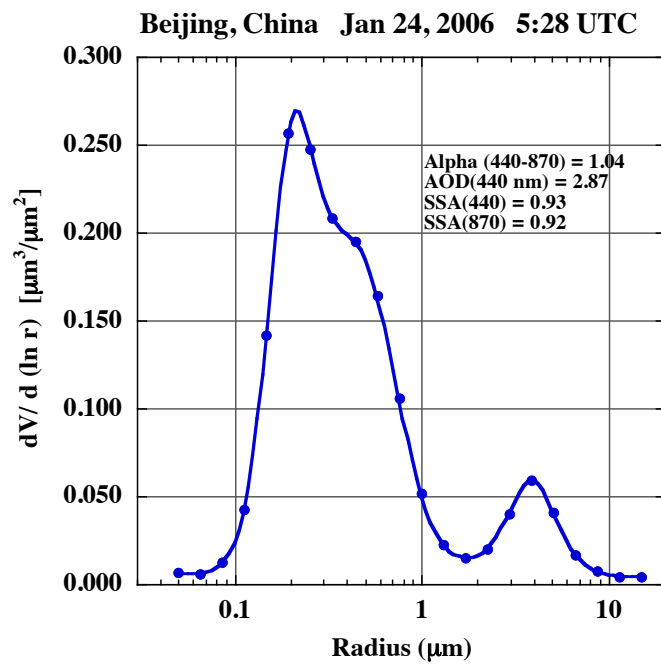


Figure 14.

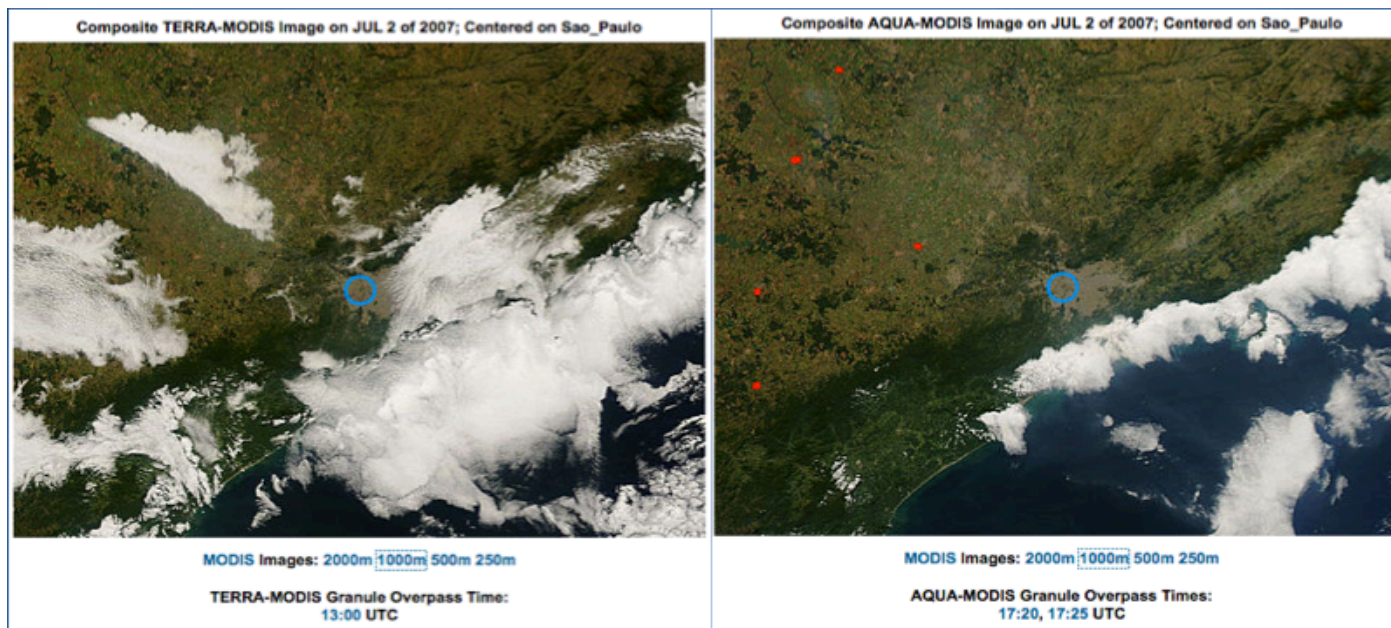


Figure 15a.

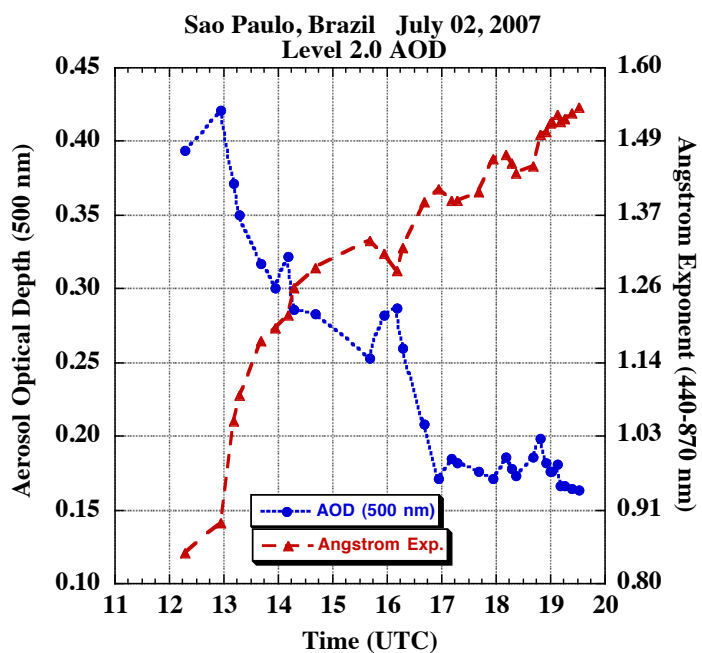


Figure 15b.

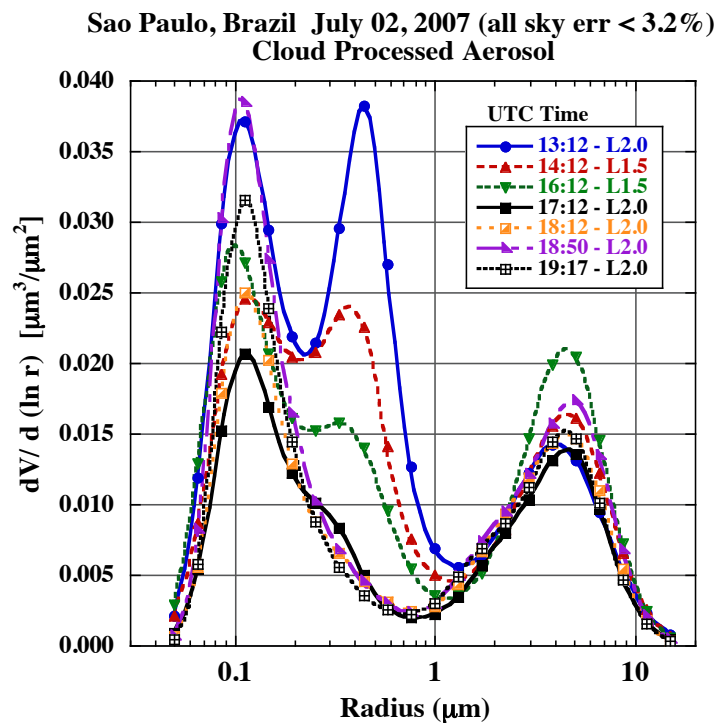


Figure 15c.

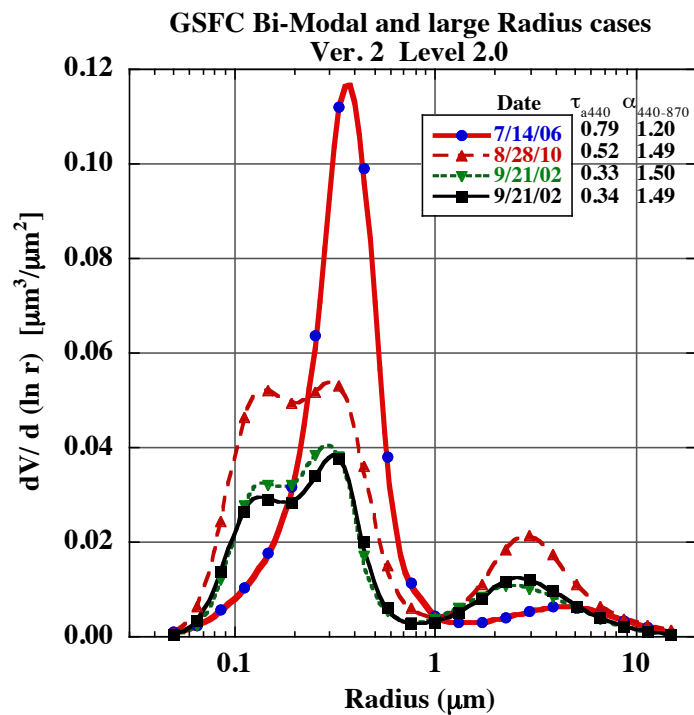


Figure 16.

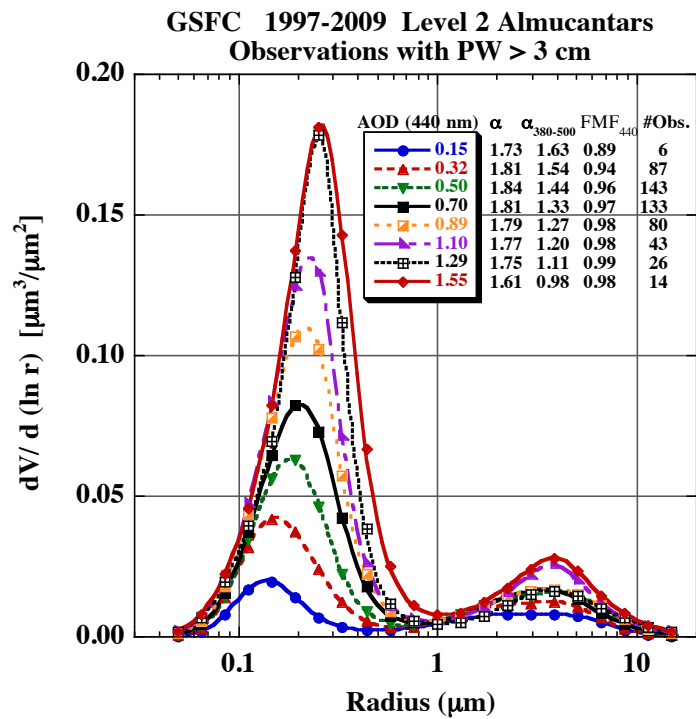


Figure 17a.

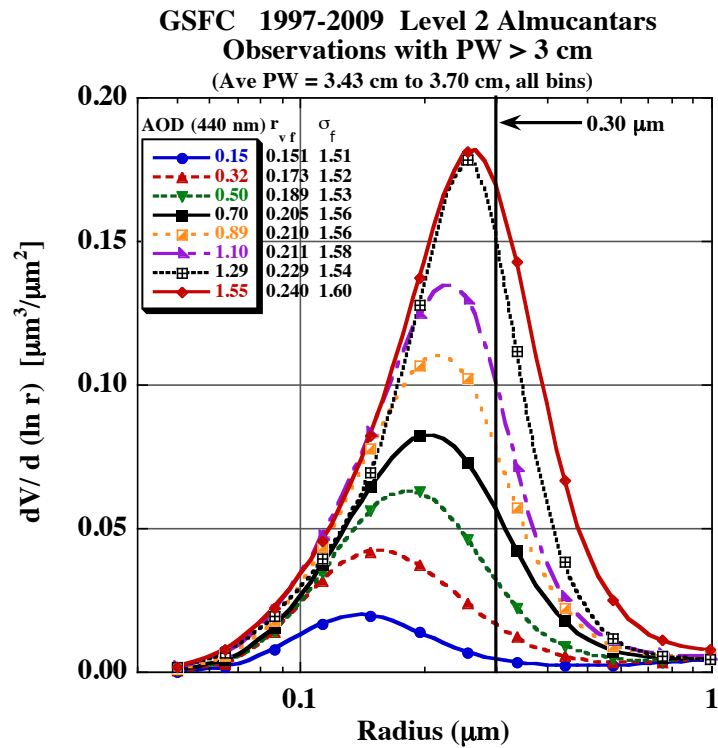


Figure 17b.